What Is CBCT and How Does It Work?

2

Ruben Pauwels

Contents

2.1 **Introduction** 13
2.2 **Stages of CBCT Imaging** 13
2.2.1 Image Acquisition 13
2.2.1.1 X-ray Source 13
2.2.1.2 Projection Geometry 15
2.2.1.3 Image Detector 17
2.2.2 Image Reconstruction 19
2.2.2.1 Pre-processing 20
2.2.2.2 Reconstruction 20
2.2.3 Grey Values vs. Hounsfield Units 22
2.3 **Comparison to Multi-Detector Computed Tomography (MDCT)** 25
2.4 **Unit Configurations** 27
2.4.1 Patient Orientation 27
2.4.2 Functionality 27
2.4.3 Volume Acquisition 28
2.5 **Technical Parameters** 29
2.5.1 Image Quality 29
2.5.1.1 Spatial Resolution 30
2.5.1.2 Contrast Resolution 30
2.5.1.3 Noise 31
2.5.1.4 Artifacts 31
2.5.1.5 Geometric Accuracy 32
2.5.2 Exposure Parameters 32
2.5.2.1 Equipment-Dependent Factors 32
2.5.2.2 Operator-Dependent Factors 35
2.5.3 Projection Images 37
2.5.4 Rotation Angle 38
2.5.5 Field of View 39
2.6 **Future Technical Developments** 40
2.7 **References** 41

R. Pauwels, Ph.D.
Department of Radiology, Faculty of Dentistry, Chulalongkorn University, Bangkok, Thailand

OMFS-IMPATH, Department of Imaging & Pathology, Biomedical Sciences Group, KU Leuven, Leuven, Belgium
e-mail: ruben.pauwels@kuleuven.be, pauwelsruben@hotmail.com

2.1 Introduction

In this chapter, the technical principles of cone beam computed tomography (CBCT) are described. Maxillofacial CBCT imaging is perhaps the most significant advance in dental imaging since rotational panoramic radiography. At the time of writing, there are more than 50 CBCT models available for clinical use worldwide (Nemtoi et al. 2013). Although there are several similarities between these models, they can differ considerably in terms of imaging hardware, exposure parameters and image reconstruction and processing.

2.2 Stages of CBCT Imaging

The production of CBCT images occurs in two stages, each with sequential phases: *image acquisition*, comprising X-ray exposure and detection, and *image reconstruction* (Fig. 2.1).

2.2.1 Image Acquisition

2.2.1.1 X-ray Source

CBCT scanners use a conventional X-ray source, consisting of a vacuum tube (Fig. 2.2) containing a cathode and anode. A filament at the cathode is heated by a large current, leading to the release of

W.C. Scarfe, C. Angelopoulos (eds.), *Maxillofacial Cone Beam Computed Tomography*,
https://doi.org/10.1007/978-3-319-62061-9_2

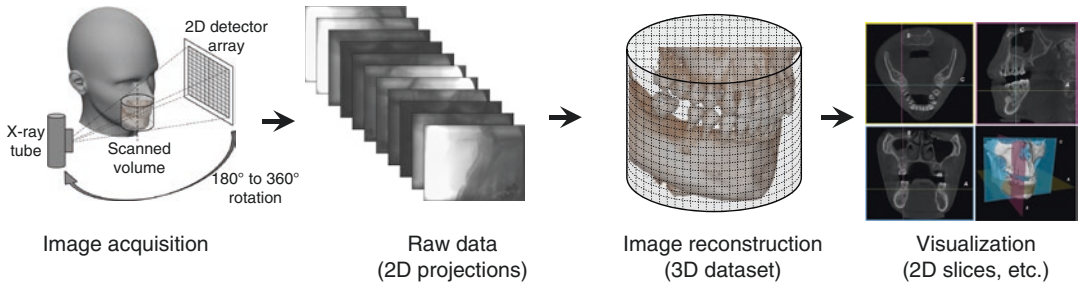

Fig. 2.1 Schematic diagram showing the stages of CBCT image production. During a 180°–360° rotation of the X-ray tube and detector, multiple planar *basis projections* (raw data) are acquired. The raw data is then reconstructed into a volumetric dataset (primary reconstruction), which is subsequently reformatted as sequential, contiguous orthogonal slices (secondary reconstruction). The data may be further reformatted (e.g., volume rendering, curved reformatting, maximum intensity projection). Partially adapted from Pauwels et al. (2015a) under the British Institute of Radiology's License to Publish

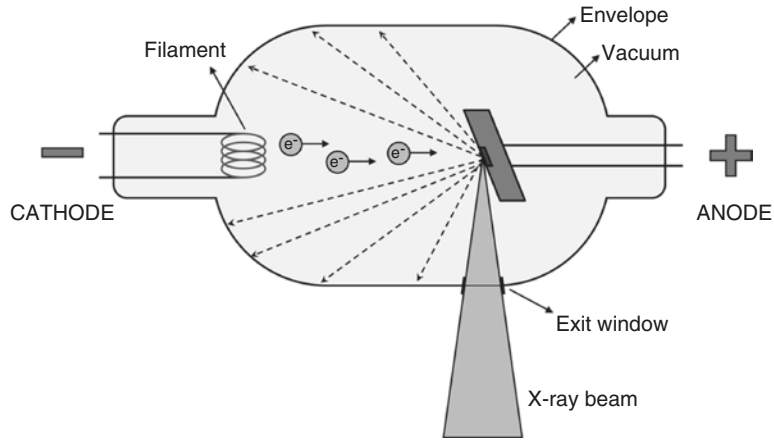

Fig. 2.2 Schematic diagram of the components of an X-ray tube. Electrons are released from the filament at the cathode and accelerated to the focal spot (*dark grey*) within the anode due to a high tube voltage. After electrons hit the anode material at the focal spot, part of the energy is released as X-rays. Figure reproduced from Pauwels et al. (2015a) under the British Institute of Radiology's License to Publish

electrons through a process known as *thermionic emission*. These electrons are accelerated across a small gap to a small area of the anode (i.e., focal spot), composed of a high-density material such as tungsten. The degree of acceleration is determined by the potential difference between the cathode and the anode, created by a high tube voltage. Collision between the accelerated electrons emitted from the cathode and orbital electrons in the anode reduces the kinetic energy of the former electrons, and energy is released through the law of conservation of energy. While most of this energy is lost as heat, a small amount is released as electromagnetic radiation in the X-ray spectrum through a process called *Bremsstrahlung* (literally (German) "braking radiation"). In addition, X-rays at specific energy levels (*characteristic X-rays*) are produced when inner-shell electrons are ejected in the anode material, after which outer-shell electrons lose energy in the form of specific X-ray emission as they occupy an inner shell. X-rays generated in an X-ray tube exhibit a wide range (spectrum) of energies, with the maximum energy determined by the tube voltage (kV) (Fig. 2.3).

X-rays generated at the focal spot diverge in all directions. Those X-rays not directed towards the detector are blocked before exiting the tube.

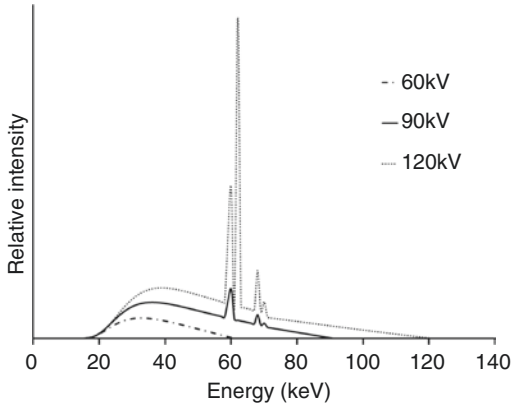

Fig. 2.3 Graph of relative intensity versus energy (X-ray spectra) for three representative tube voltages. Filtration is 2.5 mm aluminum in all cases. An increased kV results in an increased mean (shift to the *right*) and maximum (*x-axis intercept*) X-ray energy as well as an increased total intensity (*area under the curve*). Characteristic X-ray peaks are shown at fixed energy levels (i.e., for tungsten anodes: at approx. 58 keV, 53 keV, 67 keV, and 69 keV). Spectral curves were plotted using data from Birch and Marshall (1979). Figure reproduced from Pauwels et al. (2015a) under the British Institute of Radiology's License to Publish

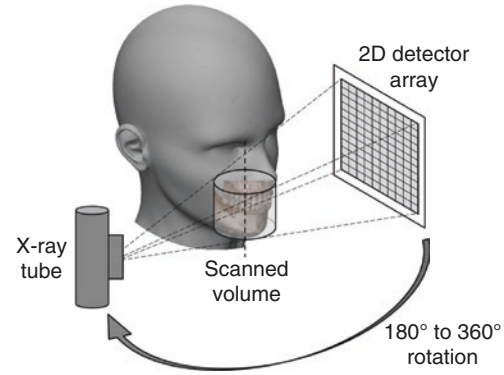

Fig. 2.4 Schematic representation of dental and maxillofacial CBCT geometry demonstrating a cylindrical scanned volume acquisition centered with the FOV size and position determined by the region of interest. Figure reproduced from Pauwels et al. (2015a) under the British Institute of Radiology's License to Publish

This is achieved by shielding surrounding the X-ray tube (tube housing) as well as high-density X-ray blockers called *collimators,* precisely restricting the aperture. Most CBCT models use rectangular collimation, resulting in a pyramid-shaped beam. Circular collimation, resulting in an actual "cone" beam, is mainly used on earlier units to correspond with the circular shape of image intensifier detectors.

2.2.1.2 Projection Geometry

In CBCT, image acquisition is performed through a single partial (≥180°) or full (360°) rotational scan of an X-ray source and a reciprocating 2D flat detector array. The axis of rotation of this configuration is centered at a certain region of interest (ROI) within the patient's head (Fig. 2.4). Throughout the rotation, a divergent pyramidal- or cone-shaped beam of X-rays is directed towards the detector on the opposite side, with the field of view (FOV) being determined by the physical collimation applied. During the rotation, many sequential 2D projection images (typically a few hundred) are acquired, each covering the FOV from a slightly different horizontal angle. These image projections constitute the raw data and are individually referred to as *basis, frame, projection, or raw images*. Because X-ray beam projections incorporate the entire FOV, only one rotational sequence (or, at the very least, half a rotation) of the gantry is necessary. The beam geometry in CBCT differs from that of multi-detector CT (MDCT), which uses a fan-shaped X-ray beam with a simultaneous translation of the patient table (gantry) and rotation of the X-ray source and detector, resulting in a helical trajectory (Fig. 2.5).

In the most basic CBCT configuration, the central ray of the X-ray beam from the generator is directed through the middle of the FOV and the transmitted, non-attenuated radiation for this central ray is projected perpendicular to the middle of the area image receptor on the opposite side. In maxillofacial CBCT noncentral rays are incident on the detector at a non-perpendicular angle. In MDCT (Fig. 2.5) the detectors are configured along an arc, assuring that the X-ray beams are incident to each detector at 90°. While divergent projection angles in CBCT can be accounted for during image reconstruction, image quality is typically optimal at the center of the FOV.

Modified Geometric Configurations

Several modified geometric configurations have been incorporated into various CBCT devices.

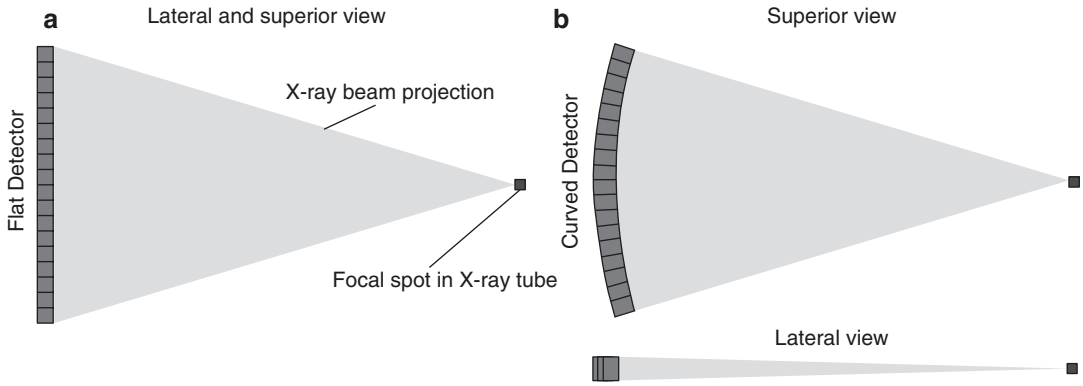

Fig. 2.5 Schematic demonstrating the difference between cone beam (**a**) versus "fan beam" (**b**) projection geometry used in CBCT and MDCT units, respectively. In CBCT, the beam is collimated as a *cone or pyramid*, and a 2D detector array is used to capture the raw data; thus, a single rotation suffices to reconstruct the FOV. In MDCT, a *fan-shaped* beam is used in concordance with an arc of detectors, resulting in the FOV being captured as a sequence of axial slices. Current MDCT units use several rows of detectors such that the X-ray beam is no longer fan-shaped but pyramid-shaped, with the divergence of the beam determined by the width and number of detector rows

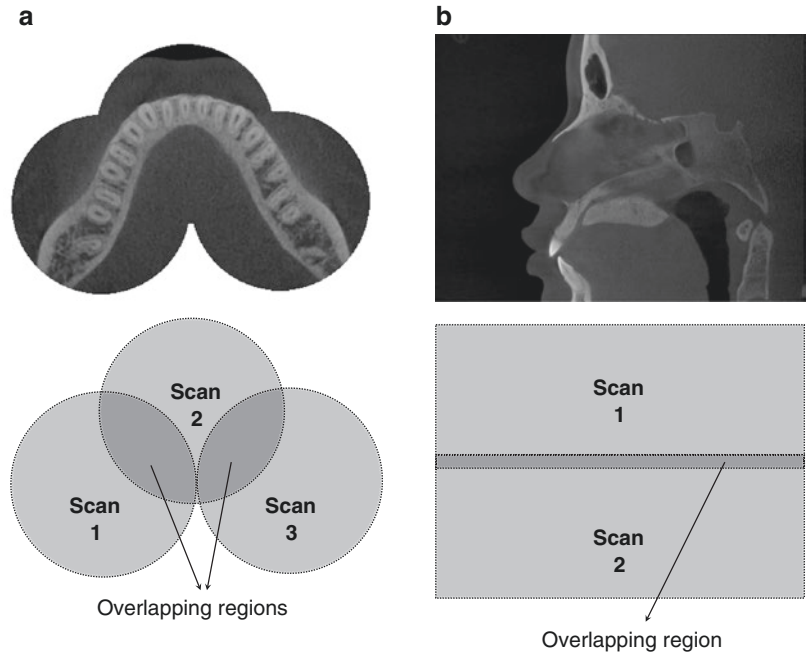

Fig. 2.6 Schematic (*lower* diagrams) and actual representative datasets (*upper* images) demonstrating *horizontal* (**a**) and *vertically* (**b**) stitched CBCT FOVs from separate sequential scans

Volumetric Stitching

One method involves obtaining data from two or more separate scans, superimposing partially overlapping CBCT data volumes through a process called *image registration* (or mosaicing) and fusing the adjacent image volumes (*stitching* or *blending*) to create a larger volumetric dataset either in the horizontal or in the vertical dimension (Fig. 2.6). This process is usually performed automatically by the CBCT software. The disadvantage of stitching overlapped regions is that such overlapped regions are exposed twice (i.e., over-scanned), resulting in doubling the radiation dose to such regions.

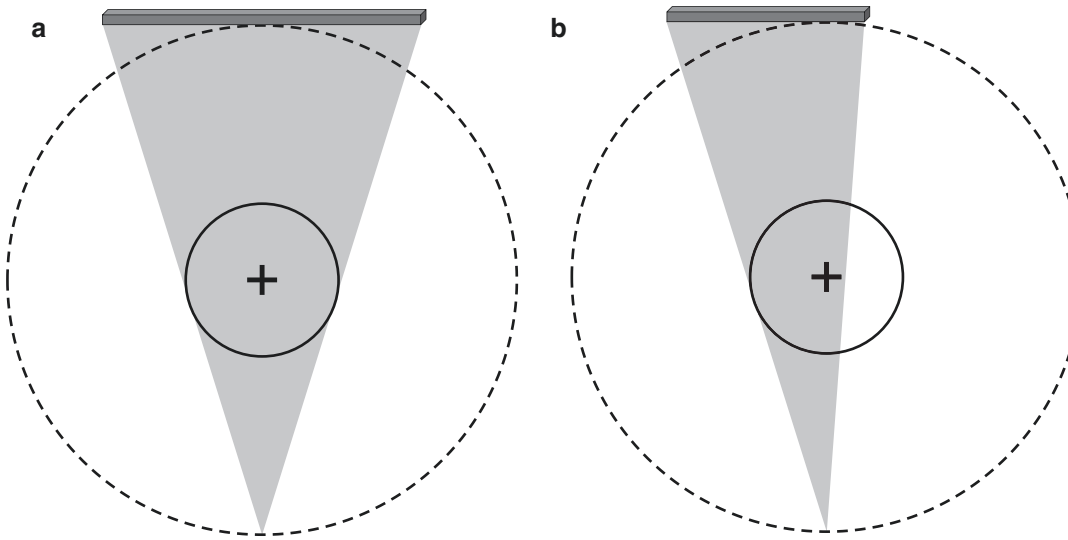

Fig. 2.7 Schematic representing conventional (**a**) and off-axis (**b**) CBCT exposure geometry in the *axial plane*. The *inner* (*solid*) *circle* denotes the FOV; the *outer* (*hashed*) *circle* shows the trajectory of the X-ray tube and detector. In the conventional geometric arrangement (**a**), the central ray of the X-ray beam from the focal source is directed through the middle of the object (+) to the center of the detector. In the off-axis geometry (**b**), only part of the FOV (at least 50%) is covered at any given exposure. An off-axis geometry allows for the use of a smaller detector for a given FOV size

Horizontal Off-Axis Geometry

A second method involves positioning of the X-ray tube and detector eccentrically to the rotational center of the FOV (isocenter) to provide an off-axis geometry (Fig. 2.7). In this configuration, the detector is offset to an asymmetrically collimated beam. As a result, only a portion of the FOV is scanned for a full 360° rotation, whereas other portions of the FOV are scanned for angles between 180° and 360° (Figs. 2.8 and 2.9).

Vertical Off-Axis Geometry

A third modified geometric configuration involves alteration of the X-ray beam projection angle in the vertical dimension (cranio-caudal plane) (Fig. 2.10). The normal cross section of X-ray beam in the vertical dimension is an isosceles triangle; thus, X-rays hit the detector perpendicularly in the central axial plane (i.e., the cranio-caudal mid-point of the FOV). Image quality is highest in this plane and slightly decreases towards the upper and lower borders of the FOV (i.e., with increasing beam divergence). If the main region of interest is expected not be in the central axial plane (e.g., a maxillofacial scan, with the main region of interest being the dentoalveolar area), optimal image quality in that region can be achieved using a scalene triangular beam shape.

2.2.1.3 Image Detector

CBCT units use either an image intensifier (II) or one of several types of flat panel detectors (FPD) as the image detector (Fig. 2.11).

- **II based systems.** Using this technology, the attenuated X-ray beam is converted into electrons. These electrons are then amplified before being reconverted into photons, which are recorded using a charge-coupled device (CCD). Currently, few CBCT units incorporate II detectors. These systems tend to be relatively large and most frequently result in circular basis image areas (spherical volumes) rather than rectangular ones (cylindrical volumes). Furthermore, they are prone to geometric distortion and have a relatively narrow dynamic range (i.e., difference between the highest and lowest detectable signal).
- **Indirect FPD systems.** An indirect system consists of two components: a scintillator

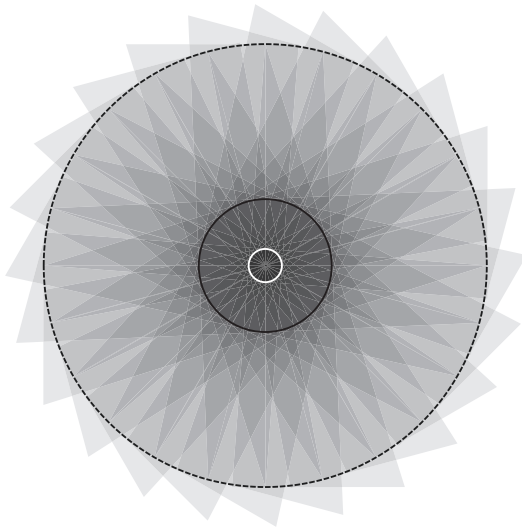

Fig. 2.8 Schematic representing the radiation coverage distribution within a rotational arc (*outer circle*) using the off-axis geometry shown in Fig. 2.7 with 24 projections. The *outer* (*hashed*) *circle* represents the trajectory of X-ray tube and detector. The *inner* (*solid*) *circle* represents the FOV. *Darker grey shades* correspond to an increased coverage. The central region of the FOV (*white circle*) is scanned through 360°. Other areas of the FOV are scanned at rotation arcs varying from 180° to 360°. The *outer edge* of the FOV (*dashed circle*) is scanned for 180°

medium which converts X-ray radiation into visible light and a photon detector which converts light into an electrical signal, which can then be digitized (Fig. 2.11). The scintillator used in CBCT is typically cesium iodide (CsI). Below the scintillator layer, FPDs comprise a thin film photodiode/transistor matrix in a 2D pixel array. Read-out of the electrical signal is done using complementary metal oxide semiconductors (CMOS) or amorphous silicon (a-Si) thin film transistors (TFT). Quality factors such as detector size, pixel size, electronic noise, sensitivity, and read-out speed depend on the technology and technical specifications of the detector.

- **Direct FPD systems.** Direct X-ray conversion detection systems (e.g., photon counting) are being developed for CBCT and have been used experimentally. FPD systems currently comprise an amorphous selenium (a-Se), cadmium telluride (CdTe), or cadmium zinc telluride (CdZnTe) photoconductor, which converts X-ray photons into an electrical charge, directly connected to a TFT or CMOS

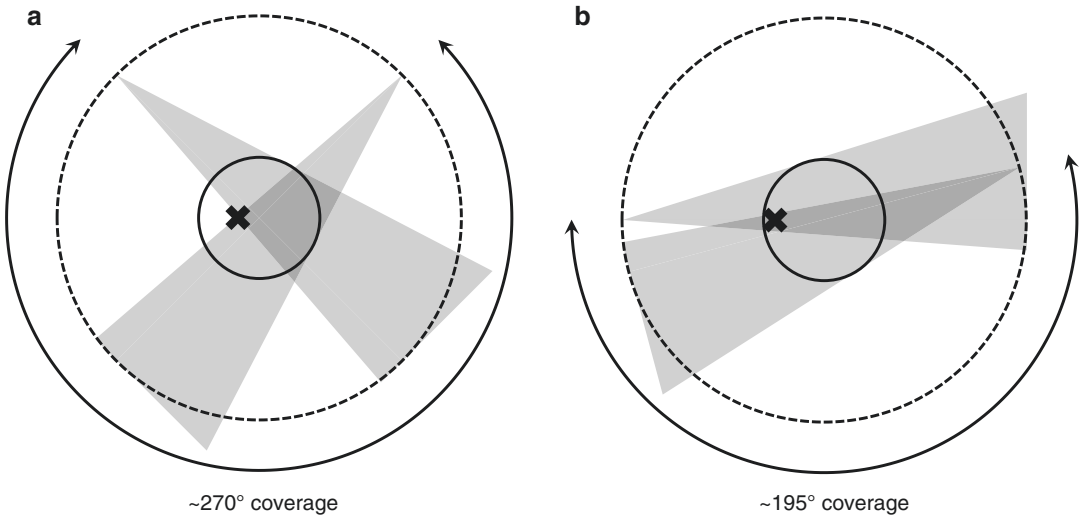

Fig. 2.9 Schematic showing the dependence of FOV coverage on location for off-axis X-ray beam projections. The trajectory of X-ray tube and detector (*hashed circle*) and FOV (*solid circle*) are shown for the off-axis geometry shown in Fig. 2.7. The start- and end-angles of the X-ray beam for which a location within the FOV (*black cross*) is covered, rounded to 15° (24-projection geometry) is shown, for a point close to the *center* of the FOV (**a**) and a point close to the *edge* (**b**). Points closer to the center of the FOV are covered using a wider rotation arc than points closer to the edge of the FOV, resulting in improved image quality closer to the center

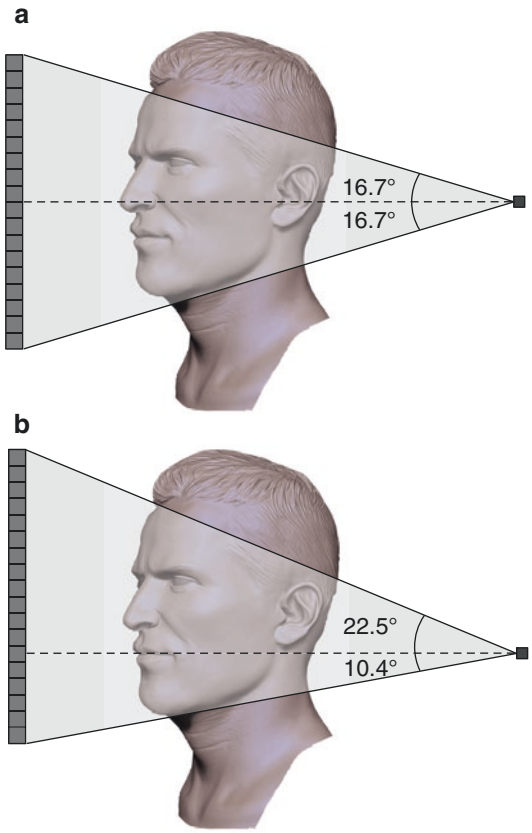

Fig. 2.10 The normal cranio-caudal geometric configuration of the X-ray beam projection (**a**) is an *isosceles triangle*, with the *central plane* of the beam (*hashed line*), at which image quality is optimal, projected perpendicular to the detector and coinciding with the center of the FOV. The use of a *scalene triangular* beam X-ray projection geometry (**b**) shifts the central plane coincides with the center of the FOV. Image quality will be highest in this plane to the area of highest diagnostic interest, usually the dentoalveolar region. (Adapted from Molteni (2013); 3D head model image courtesy of Rodrigue Pralier)

panel (Fig. 2.11). Images from direct detector systems are inherently less unsharp than those from indirect detector systems, as the latter involves a conversion to visible light, which is laterally spread between detector elements.

For each projection image during acquisition, the detector receives incident X-ray photons, collects a charge proportionally to the X-ray intensity at a given point, and sends a signal to the computer. As rotation is usually performed within times equivalent to panoramic radiography (typically 15 –20 s, although scan times below 10 s or above 30 s are possible), each of the hundreds of projection images is acquired and transmitted within milliseconds. The speed with which a detector performs this acquisition is called the *frame rate*. The limited frame rate of FPD detectors used in CBCT, as well as the potential afterglow effect if consecutive projections are acquired with a too short lag period, limits the minimal exposure time needed in CBCT.

FPD have limitations in their performance including linearity of response to the radiation spectrum, lack of uniformity of response throughout the area of the detector, and possible nonfunctioning pixels (see also Sect. 2.2.2.1). To overcome this, units with FPDs should be recalibrated periodically.

An important property of X-ray detectors is their *pixel size* (i.e., the physical size of individual detector elements), which is a principal determinant of resolution and therefore detail of CBCT images. The theoretical spatial resolution in CBCT is dependent on the nominal pixel size of the detector array, but is reduced to some extent by other factors in the imaging chain (e.g., focal spot size, voxel size of the reconstructed image). On the other hand, detectors with smaller pixels capture less X-ray photons per detector element, resulting in increased image noise. This can be compensated for in two ways. First of all, detector elements can be binned (e.g., grouped together and considered as one element), for example, in a 2 × 2 configuration; while this reduces image noise, spatial resolution will be reduced as well. Alternatively, the tube output (and thus the patient dose) can be increased to achieve an adequate signal-to-noise ratio.

2.2.2 Image Reconstruction

In CBCT, each projection image consists of a pixel matrix with a 12- to 16-bit value (proportionate to the detected X-ray intensity) assigned to each pixel. This data is then reconstructed into a 3D volumetric dataset composed of cubical volume elements (voxels) by a sequence of software algorithms. Subsequently, orthogonal (i.e.,

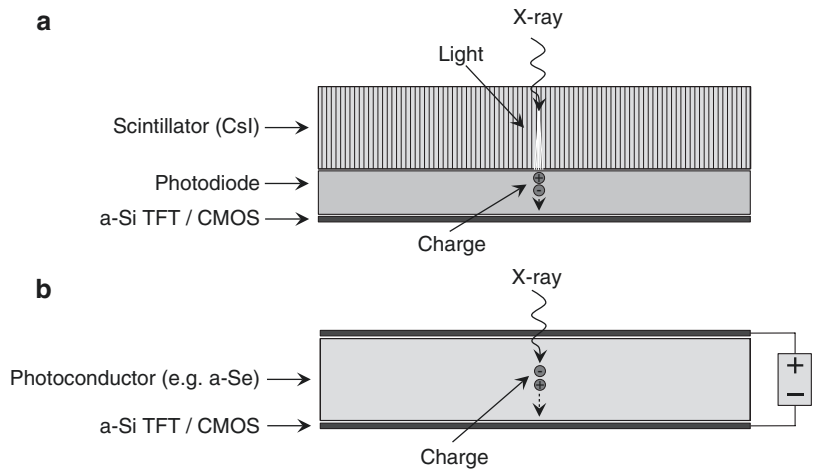

Fig. 2.11 Schematic representation of indirect (**a**) and direct (**b**) FPD systems. (Adapted from Seibert (2006), reproduced under the Creative Commons Attribution Noncommercial License)

perpendicular images in all three planes) sectioning of the volumetric dataset is provided, and additional visualizations can be created.

Reconstruction is computationally complex, so, to facilitate workflow, data is often acquired by one computer (acquisition computer) and transferred via Ethernet connection to a second computer (workstation) for processing. Reconstruction times vary depending on the acquisition parameters (voxel size, FOV, number of projections), hardware (processing speed, data throughput from acquisition to workstation computer) and software (pre- and post-processing, reconstruction algorithm) used. Reconstruction should be accomplished in an acceptable time (usually less than 5 min) to complement patient workflow. The reconstruction process consists of numerous steps.

2.2.2.1 Pre-processing

Due to spatially varying physical properties of the detector elements, as well as variations in the X-ray sensitivity of the scintillator layer, raw images from CBCT detectors have spatial variations referred to as dark image *offset* and *pixel gain* variation. The dark image offset (i.e., the detector output signal without any X-ray exposure), and its spatial variations are mainly caused by dark current of the photodiodes. Pixel gain variations are caused both by varying sensitivity of the detector elements and by deviations of the local conversion efficiency of the scintillator or direct conversion material due to, for example, slight variation in thickness or density. In addition to these spatial variations, detectors exhibit inherent pixel imperfections or defects. To compensate for these inhomogeneities, raw images require systematic offset and gain calibration as well as a *correction of defective pixels* (Fig. 2.12). Subsequently, temporal artifact correction can be applied by estimating and then subtracting the *afterglow* signal from prior projection images. This sequence of calibration steps is referred to as *detector pre-processing*.

2.2.2.2 Reconstruction

The most widely used reconstruction algorithm in CBCT is the Feldkamp (FDK) algorithm, which is a modified *filtered backprojection* (FBP) method (Feldkamp et al. 1984). Using backprojection, the total X-ray attenuation measured at a detector pixel is equally distributed to all voxels in the FOV which are traversed by the X-rays reaching that particular pixel. A simple representation of backprojection is shown in Figs. 2.13, 2.14, 2.15, 2.16, and 2.17.

Figure 2.13 shows 1D projections of a 2D image using parallel projection lines. After backprojecting, the detected attenuation value along every point of the projection line, backprojections from different projection angles can be averaged (Fig. 2.14). When a larger number of projection angles are combined, the reconstruction represents the original object more accurately

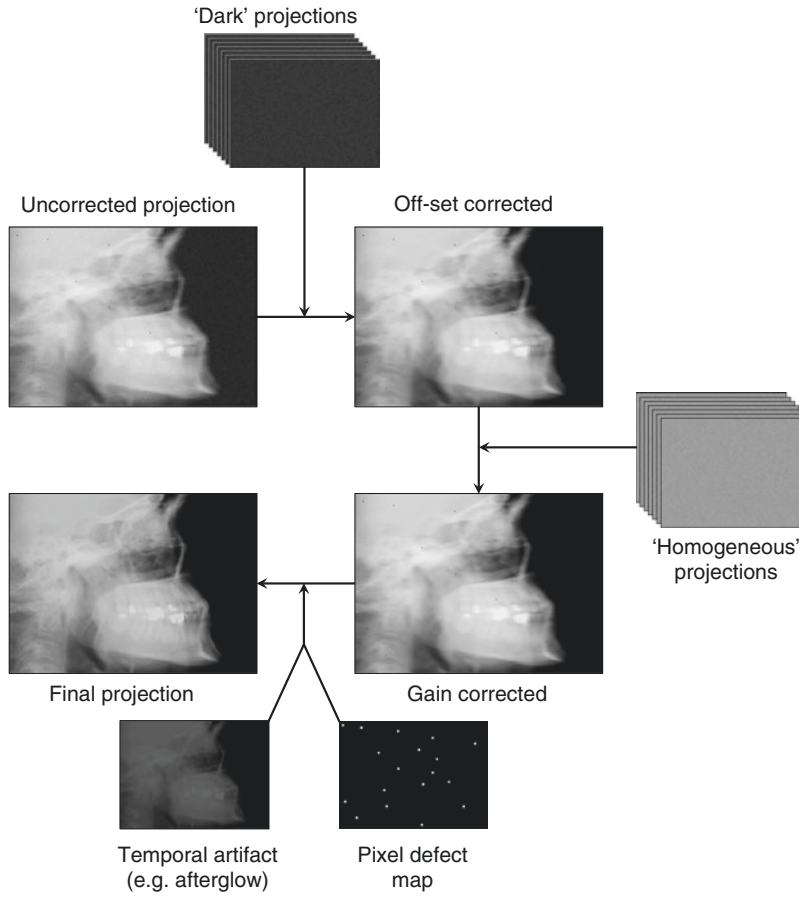

Fig. 2.12 Schematic diagram illustrating CBCT preprocessing steps. Initially, offset correction is performed by pixel-wise subtraction of an individual offset value computed by averaging over a series of *dark* images (acquired without any X-ray exposure). Next, linear gain calibration is performed, consisting of dividing each pixel by its individual gain factor. Gain factors are obtained by averaging a sequence of homogeneous exposures, which have their own sequence of *dark* images, without any object between the X-ray source and detector. Finally, defect interpolation is performed. Each pixel that shows unusual behavior, either in the gain image or in the average *dark* sequence, is marked in a defect map. The *grey* values of pixels classified as defective in this way are computed by interpolation. For flat panel detectors, there is usually an additional procedure to correct for temporal artifacts. These arise in flat detectors because both the scintillator and the read-out panel at the detector exhibit residual signals (i.e., afterglow).

(Fig. 2.15). Nonetheless, the backprojected image is a blurred representation of the original. To compensate for this, the projections can be filtered to enhance the edges (Fig. 2.16). Different filters with varying levels of sharpness/smoothness can be used (Fig. 2.17) (Pauwels et al. 2015a).

An alternative reconstruction method is *iterative reconstruction*. This is a general name for an algorithm which undergoes several repetitions (i.e., iterations) before the final reconstructed image is produced. Typically, iterative reconstruction is done by forward projecting an initial estimate (which can be a conventional FBP reconstruction, a crude model of the expected anatomy or a blank image) and comparing the result with the actual projection data. The estimate is then corrected accordingly, a new forward projection is generated and the process is repeated for a set number of iterations or until a predetermined level of agreement is found (Fig. 2.18). In MDCT, iterative reconstruction has been introduced in clinical practice by all

manufacturers, generally resulting in substantial noise reduction (and as a result, a potential mAs reduction) compared with FBP reconstruction without sacrificing spatial resolution. Also, more advanced iterative reconstruction techniques (e.g., metal artifact reduction, noise suppression) have been proposed (Beister et al. 2012). Despite its versatility, the main disadvantage of iterative reconstruction is the large amount of computation involved, which increases proportionally with the number of iterations. Therefore, in CBCT, iterative reconstruction is still largely absent in clinical practice, but is expected to become more common in the near future.

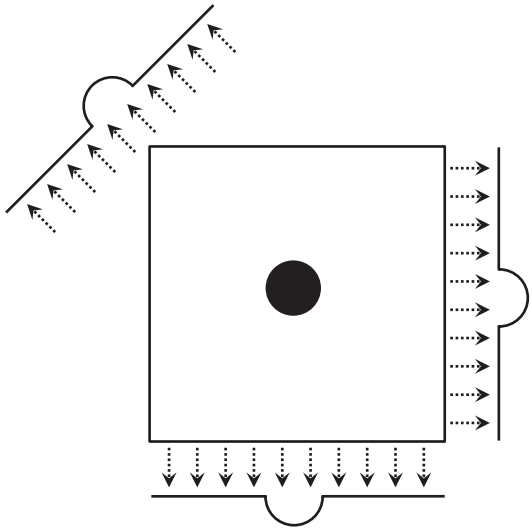

Fig. 2.13 Forward X-ray projection of a circular object using parallel projection lines

2.2.3 Grey Values vs. Hounsfield Units

CBCT images are reconstructed as a 3D stack of *voxels*, in which each voxel is assigned a *grey value* (i.e., a whole number) according to its estimated X-ray attenuation. A lower grey value corresponds to a lower attenuation, with the lowest grey values corresponding to air. Typically, grey values are distributed along a 12-bit scale, implying that 4096 possible grey values can be assigned. Extended bit depths along nominal scales up to 16 bit (with the actual bit depth typically at 13–14 bit) are used as well, although it is somewhat questionable whether image quality (esp. contrast) is improved as a result.

In MDCT, grey values can be calibrated along the *Hounsfield scale*, allowing for quantitative evaluation of attenuation. The Hounsfield scale is determined using the attenuation of air and water as calibration points, with air corresponding to

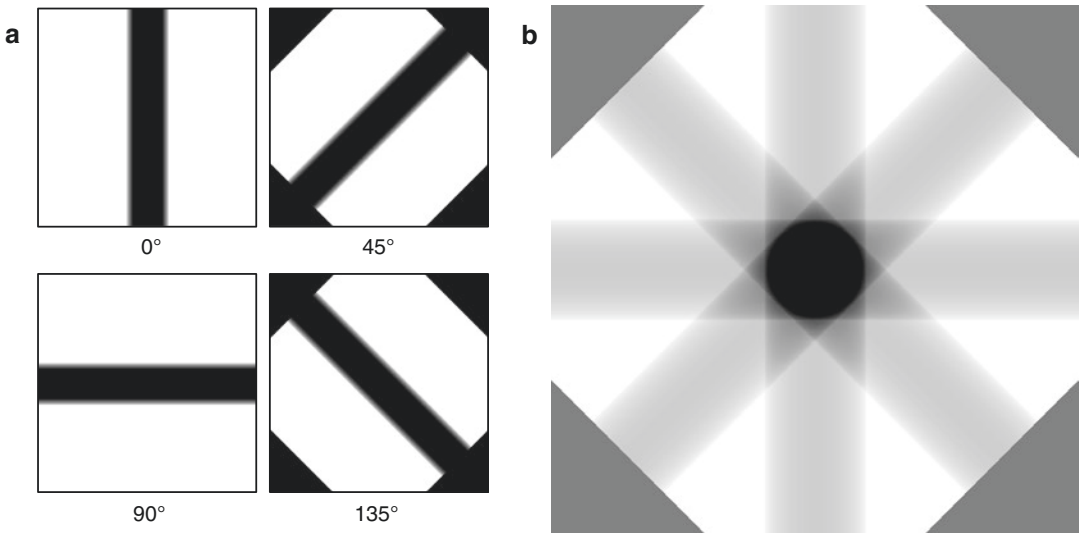

Fig. 2.14 Backprojection of the object in Fig. 2.13 from four projection angles (**a**) providing an average of the four backprojections (**b**)

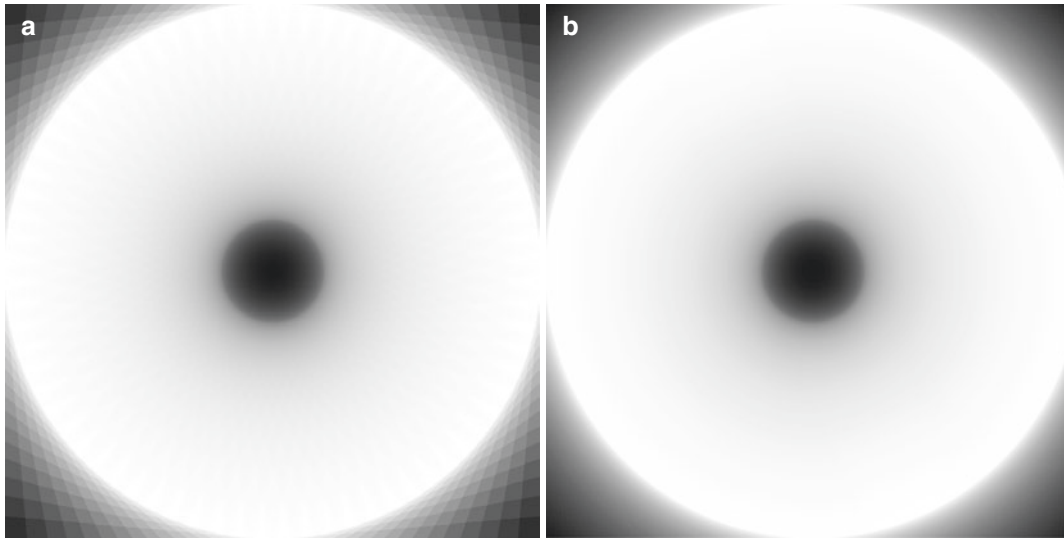

Fig. 2.15 Average of 36 (**a**) and 180 (**b**) backprojections of the object in Fig. 2.13

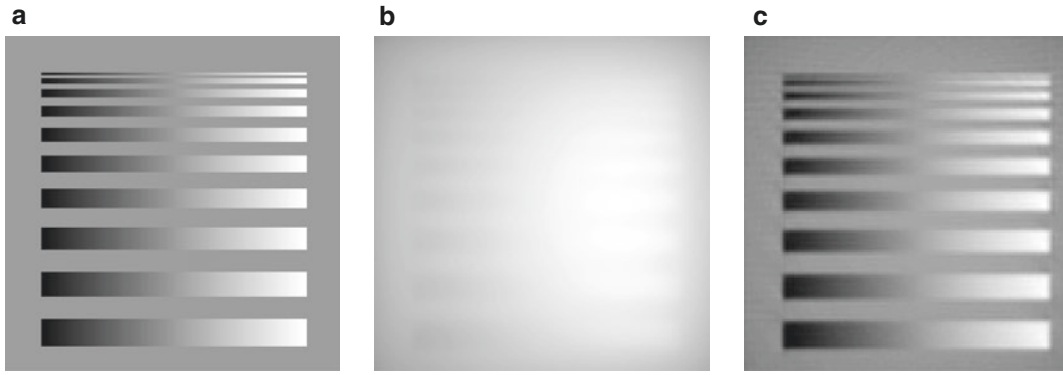

Fig. 2.16 Line pattern original image (**b**), unfiltered backprojection (**b**), and filtered backprojection (**c**)

−1000 Hounsfield units (HU) and water to 0 HU. HU calibration has several potential applications, including the discrimination of solid- and liquid-filled growths, and the estimation of bone mineral density (BMD). In CBCT, however, the use of HU is severely limited by several inherent issues regarding grey value stability. Some of the most notable issues are:

- **High amount of detected X-ray scatter.** Although uniformly distributed scatter (as well as other sources of noise) does not affect overall grey value stability, scatter can be non-uniform leading to image shading.
- **Beam hardening.** Beam hardening is the increase in mean energy of an X-ray beam passing through tissue. When not properly compensated for, it can lead to darkening in regions where the beam was "harder." As CBCT units typically operate at a lower kV than MDCT (and thus contain a higher proportion of low-energy X-rays), beam hardening is more pronounced.
- **Effect of tissues outside FOV.** The use of horizontal collimation results in the "local tomography" effect, in which asymmetrically distributed tissue is found outside the FOV. This tissue leads to varying degrees of

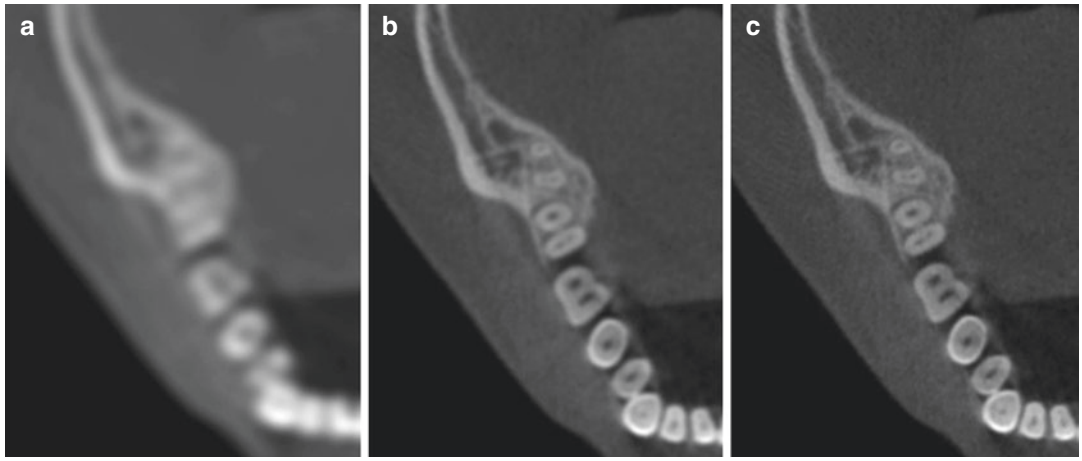

Fig. 2.17 Axial CBCT images showing the effect of different cutoff frequencies (expressed as a fraction of the Nyquist frequency) using cosine reconstruction filters (**a**) 0.2 cutoff; (**b**) 0.6 cutoff; (**c**) 1.0 cutoff. A larger cutoff frequency during filtration increases both spatial resolution and noise. (Figure reproduced from Pauwels et al. (2015a) under the British Institute of Radiology's License to Publish

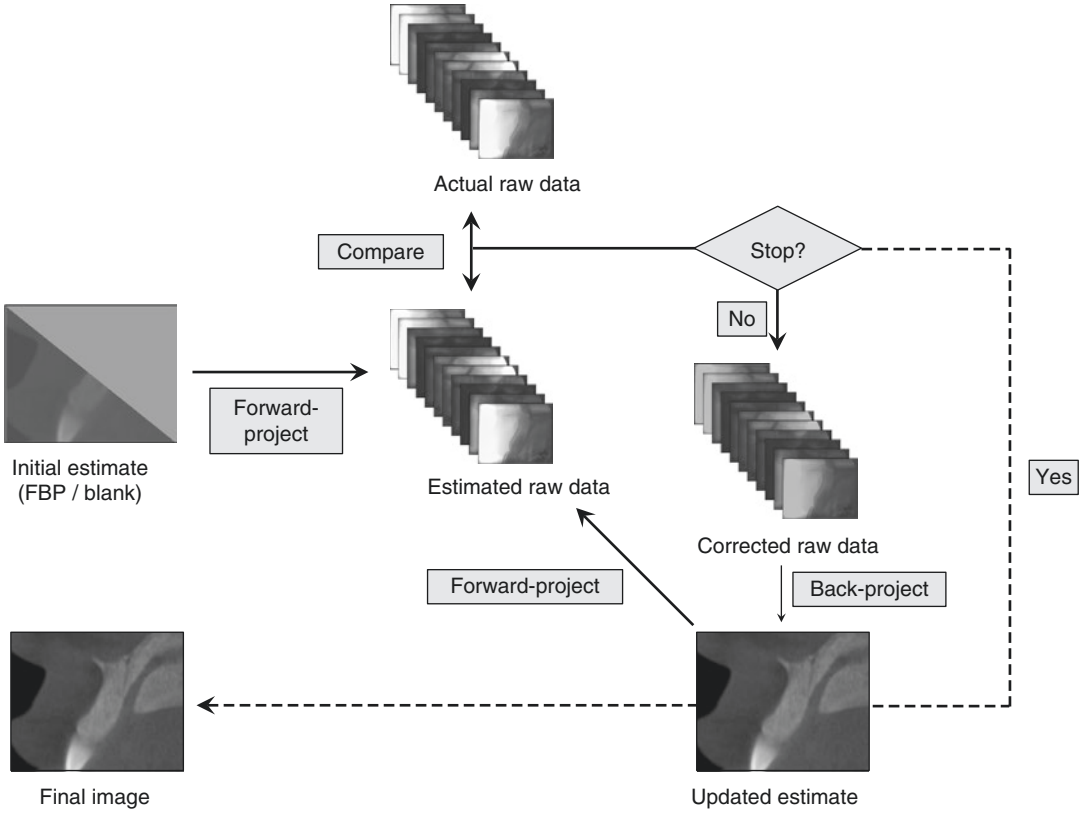

Fig. 2.18 Schematic representation of iterative reconstruction approach in CT. An initial image estimate (which can be a blank image or an FBP reconstruction) is forward-projected, and the estimated raw data is compared with the actual raw data acquired by the CT scanner. The estimated raw data is then corrected and backprojected to obtain a new image estimate. This process is repeated until sufficient agreement between the estimated and actual raw data is found, or until a fixed number of iterations has been made

added attenuation for projections acquired at different angles, and can lead to a grey value gradient (typically an anteroposterior shading for dental scans).

- **Metal artifacts.** Although metal artifacts are not exclusive to CBCT, they commonly occur in dental scans due to the large amount of metallic restorations found in the patients' dentition. Metal artifacts are manifested as dark and bright streaks and areas, close to or radiating from the metal object. The appearance and severity of metal artifacts depend on the number, size, shape, and relative locations of the metals. Because of the CBCT imaging geometry, they are mainly found in the axial plane, with a slight divergence along the z-axis depending on the X-ray beam angle.

In general, the use of grey values as HU (or in any quantitative way) should be avoided in CBCT, although it may have some limited use in controlled circumstances. A detailed description of grey value stability issues in CBCT can be found in the reviews by Pauwels et al. (2015b) and Molteni (2013). More information regarding grey value uniformity and artifacts can be found in Sect. 2.5.1.

2.3 Comparison to Multi-Detector Computed Tomography (MDCT)

The principal difference in volumetric data acquisition between CBCT and MDCT is that the latter uses a fan-shaped X-ray beam (Fig. 2.5) in a helical progression acquiring individual image slices of the FOV, which are then stacked to obtain a 3D representation. Each slice requires a separate rotation and separate 2D reconstruction. However, modern MDCT scanners use a large number of detector rows in order to increase the number of slices acquired simultaneously. Therefore, MDCT has become somewhat more akin to CBCT in terms of beam geometry, with newer models providing an increasingly divergent X-ray beam. However, there are still essential differences between the two technologies (Table 2.1). As a result, patient dose and image quality can differ considerably between CBCT and MDCT.

Patient dose from MDCT is generally higher than that of a corresponding CBCT scan (Loubele et al. 2009), as CBCT is usually associated with a lower tube output (kV, mAs) and a horizontally collimated FOV. However, low-dose MDCT protocols for implant planning, with doses overlapping with the high end of the dose range of CBCT, have been proposed (Loubele et al. 2005). As a result of recent technological innovations in MDCT, such as noise reduction through iterative reconstruction, it can be expected that scans of the hard tissues of the dentomaxillofacial region can be acquired at a very low dose using current-generation MDCTs. However, as MDCT is scarcely used in dentistry nowadays, dedicated low-dose protocols for dental applications and accompanying dose reports are lacking. In terms of image quality, as discussed in Sect. 2.5.1, CBCT images are characterized by a high spatial resolution owing to the use of small detector pixels and correspondingly small image voxels. However, contrast resolution is limited by the detector's dynamic range, and a relatively high proportion of scattered radiation at the detector, among other factors. X-ray scatter, along with the small detector pixels and image voxels and the low tube output, also results in a high image noise compared with MDCT.

While CBCT imaging is considered to be superior for visualization of small details with high anatomical contrast, it cannot be used for applications in which soft tissue discrimination is needed (e.g., characterization of tumors or cysts). In these circumstances, MDCT or magnetic resonance imaging with or without contrast is indicated. In terms of artifacts, while CBCT and MDCT are generally prone to the same types of artifacts, motion artifacts can be more pronounced in CBCT (especially when long scanning times are used). Furthermore, CBCT images can have poor uniformity of grey values due to the use of horizontal collimation and the subsequent presence of tissue outside of the FOV (see Sect. 2.5.1.4). As for metal artifacts, there are little or no reasons for differences in terms of artifact severity between CBCT or MDCT images as

Table 2.1 General similarities and differences at each stage of imaging between MDCT and CBCT

Stage	Similarities	Differences
X-ray beam shape	• Pyramid-shaped beam (albeit with different relative dimensions)	• Full coverage in MDCT in terms of beam diameter; diameter of beam is collimated to as small as 4 cm in CBCT
		• Beam divergence in CBCT at upper and lower borders of the FOV is typically larger than that of MDCT, even when many detector rows are used
		• Beam in MDCT can be narrow if few detector rows are used
Detector	• Typically, indirect X-ray detection (using scintillator, or xenon gas ionization chamber for some MDCT units)	• Different scintillator material used, typically cesium iodide in CBCT and gadolinium oxysulfide in MDCT. As a result, detector sensitivity, efficiency, dynamic range, and speed differs
	• Detector elements can be binned to increase signal-to-noise ratio (at the cost of spatial resolution)	• Image intensifier detectors used in older CBCT models
		• Flat detector used in CBCT, detector arc (with perpendicular X-ray detection throughout the FOV) used in MDCT
		• Size of detector elements can vary between central and peripheral slices in MDCT; detector pixels are uniform in size in CBCT
		• The use of a flat detector in CBCT, along with a generally short patient-detector distance, increases the proportion of detected X-ray scatter. Physical collimation between detector rows in MDCT can lead to additional scatter reduction along the z-direction
Technique factors	• kVp, mA, field of view settings determine image quality and patient radiation dose	• Certain technique factors differ: MDCT involves selection of pitch, acquired slice thickness, and pixel size, whereas CBCT involves selection of rotation arc, voxel size, and number of projection images
		• Automatic exposure control is ubiquitous in MDCT but largely absent in CBCT
		• CBCT typically operates at a lower mAs (although low-dose MDCT protocols can reach similar mAs levels)
		• Dual energy imaging possible in MDCT, but not yet implemented in CBCT
Patient preparation	• For some CBCT models, patients is supine as in MDCT	• Patient is standing or seated for most CBCT units
Patient protection	• Lead torso shield	• Extra care should be taken in MDCT with automatic exposure control, as the use of shielding in the primary beam may lead to a severe increase in tube output
	• Thyroid shield is desirable, especially for maxillary scans. For lower jaw or maxillofacial scans, potential metal artifacts should be considered	
Exposure	• Patient informed to keep still	• Scan time varies from 5 s to greater than 30 s in CBCT whereas modern MDCT scanners allow for sub-second scans; thus, motion artifacts are more likely to occur in CBCT
		• Patient is stationary in CBCT (with the exception of dual acquisition in which the chair may move between scans). In MDCT, the table moves continuously during exposure
Image viewing	• Image must be reconstructed before viewing (30 s–>10 min)	• Secondary, multi-planar and other reformatted images are of almost equal resolution in CBCT because of isotropic voxels. In MDCT, coronal and sagittal slices can have poorer resolution than axial images (depending on slice thickness and pitch)
	• Images are conventionally reconstructed using a type of filtered backprojection	• Advanced reconstruction techniques (e.g., iterative reconstruction, noise reduction, metal artifact reduction) common in MDCT but not yet in CBCT
	• Basic image processing possible, e.g., contrast, brightness, zoom, filtering	

a result of fundamental differences between the imaging techniques. Different appearances of metal artifacts between CBCT and MDCT can be attributed to scanner and reconstruction factors (e.g., beam energy, calibration of the grey value histogram, beam hardening correction, and other metal artifact suppression techniques).

2.4 Unit Configurations

In 2013, it was determined that 47 CBCT models from 20 manufacturers were used in Europe (Nemtoi et al. 2013). At the time of writing, over 50 models are found worldwide. There are a few pronounced differences in terms of configuration between these systems. They can be distinguished based on patient orientation during image acquisition, whether they are hybrid systems with panoramic (and cephalometric) functionality, and on the available FOV options.

2.4.1 Patient Orientation

Most CBCT units operate with the patient in a *standing or sitting* position. Standing/seating units are typically compact (i.e., small physical footprint), allowing them to be placed in private dental clinics or other environments where little space is available. Few CBCT models are available where the patient is scanned in the supine position, as in MDCT. Furthermore, different head restraint mechanisms are used, as patient motion may limit spatial resolution. Combinations of head rests, chin rests or bite blocks, straps and lateral fixation are currently used.

2.4.2 Functionality

CBCT systems can be stand-alone or hybrid systems. Hybrid or multi-modal systems combine digital panoramic and/or cephalometric radiogra-

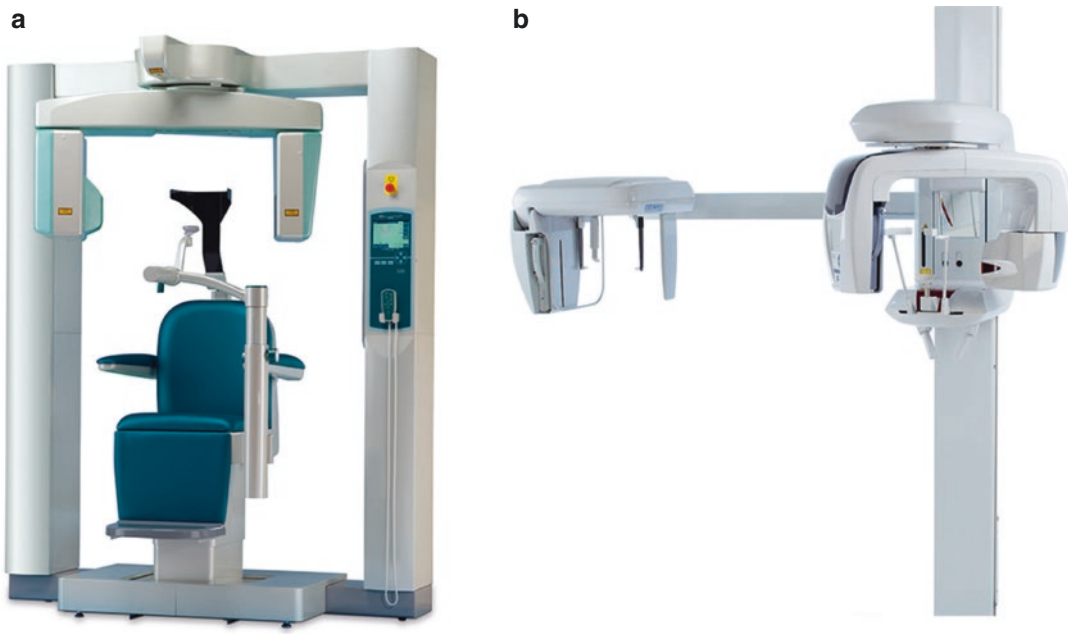

Fig. 2.19 Examples of stand-alone (**a**) 3D Accuitomo 170, (J. Morita, Osaka, Japan) and all-in-one hybrid unit configurations with CBCT, panoramic and cephalometric imaging (**b**) Veraviewepocs 3D R100, (J. Morita, Osaka, Japan). Images courtesy of J. Morita, Osaka, Japan

phy with CBCT in a single equipment (Fig. 2.19). The use of hybrid systems can be cost- and space-efficient.

2.4.3 Volume Acquisition

CBCT units can be assigned into four broad categories based on the vertical and horizontal dimensions of the FOV (Fig. 2.20):

- **Large (Maxillofacial).** Covers most of the craniofacial skeleton, at least from below the hard tissue of the chin to the nasion. Usually greater than 15 cm in any dimension.
- **Dentoalveolar (both jaws)**. Usually 8 cm or more in diameter and height.
- **Single jaw/dual TMJ.** Can cover a single full jaw (excl. ramus for mandibular scans) or both temporomandibular joints. Wide in diameter (≥ 10 cm, or ≥ 14 cm if used for TMJs) but small in height (4–6 cm).
- **Small (localized)**. As small as 3 cm in any dimension, covering localized regions such as 2–4 teeth and surrounding alveolus or a single temporomandibular joint.

As discussed in Chap. 7, the FOV size is one of the primary determinants of radiation dose; thus, proper selection of the FOV according to the diagnostic task is paramount. This also implies that the purchase of a CBCT machine should take its intended use (and the minimal and maximal FOV size required to cover this intended use) into account.

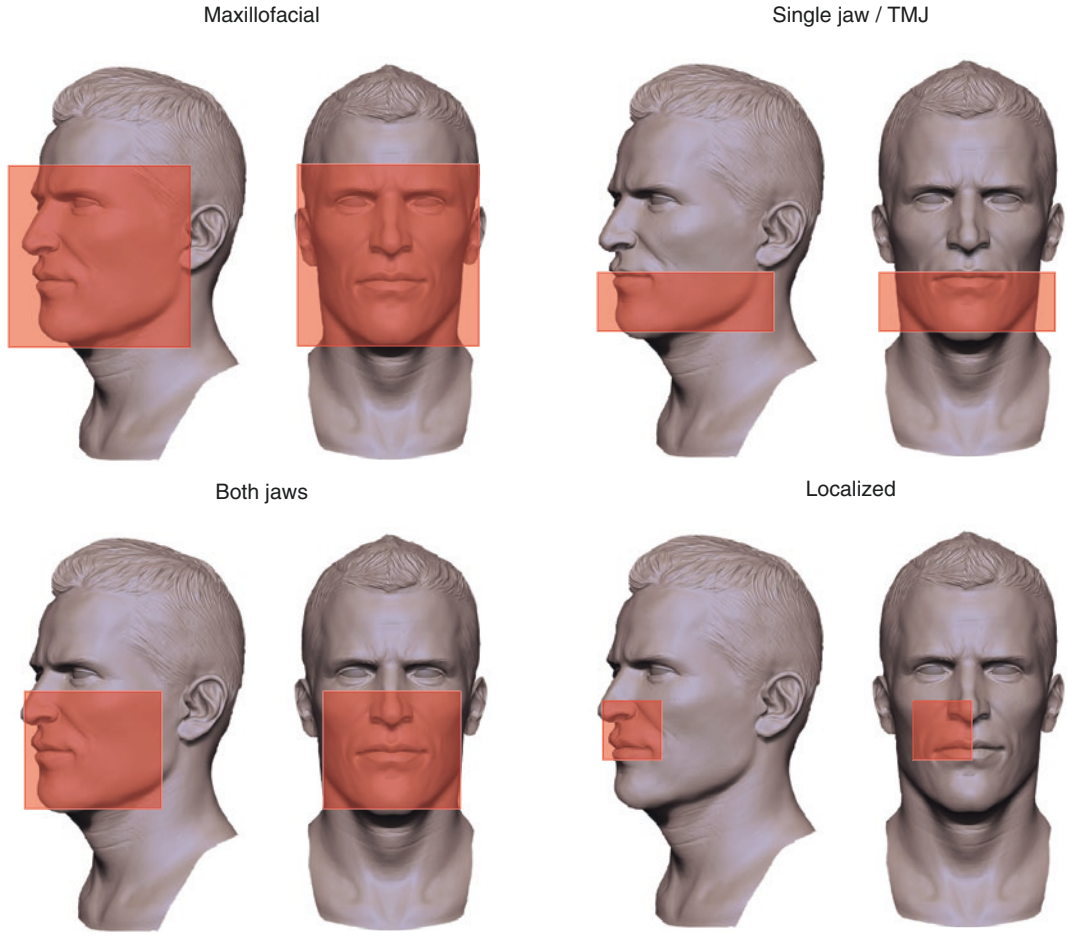

Fig. 2.20 Examples of four broad categories of FOV sizes used in dental and maxillofacial CBCT. 3D head model images courtesy of Rodrigue Pralier

2.5 Technical Parameters

While CBCT units are relatively simple to operate, they exhibit wide differences in technical parameters available to the operator. CBCT users must be able to choose an appropriate imaging protocol (i.e., a selection of specific technical parameters) for each patient to *optimize image quality and minimize radiation dose* for a specific imaging task. Therefore, practitioners and operators using CBCT must have theoretical knowledge and a practical understanding of the effects of available technical parameters on image quality and radiation dose. Readers are referred to Chaps. 5 and 7 for more details regarding radiation dose and radiation protection.

2.5.1 Image Quality

Image quality can be described using four fundamental parameters: *spatial resolution, contrast resolution, noise, and artifacts* (Fig. 2.21). Additionally, *geometric accuracy/distortion* can

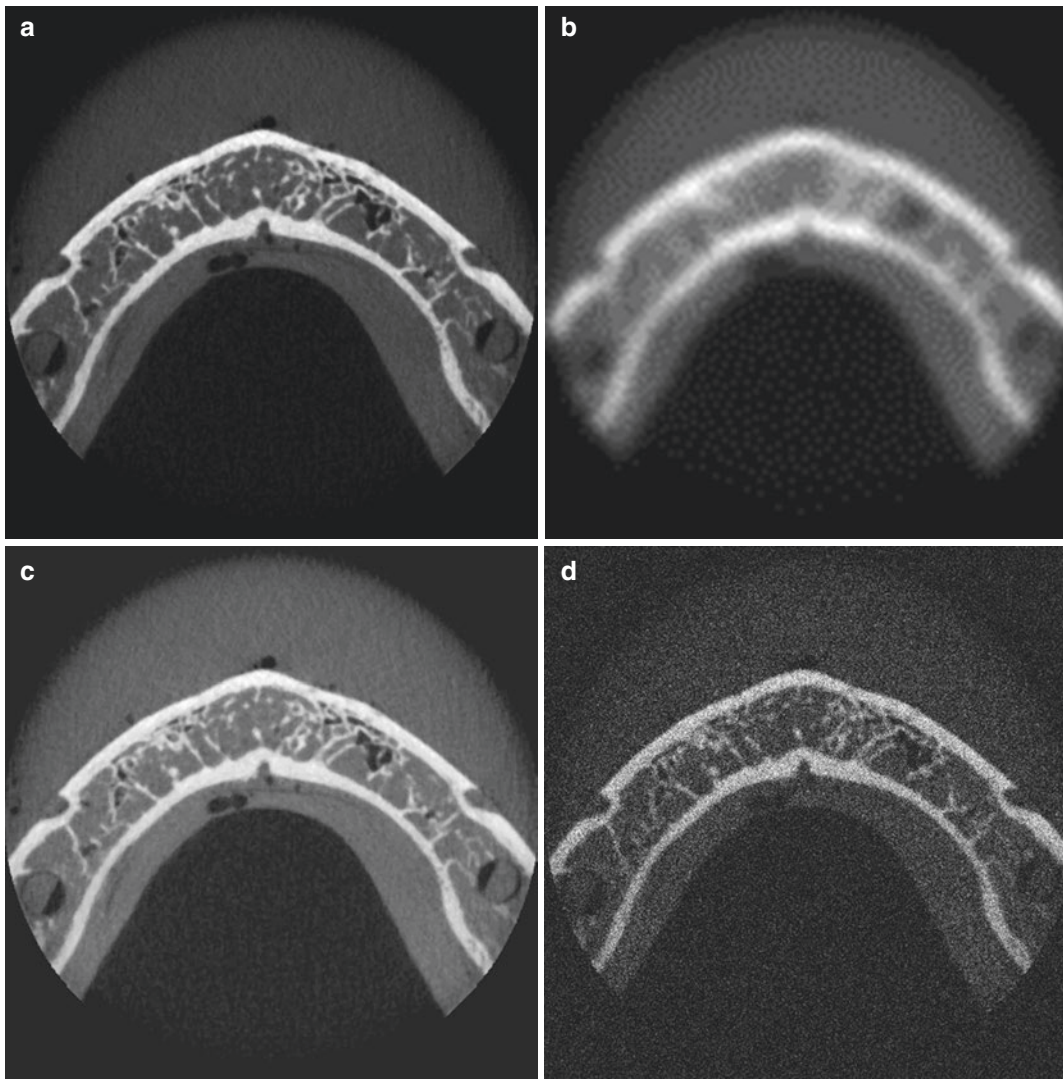

Fig. 2.21 Representative axial CBCT images demonstrating visual differences observed with changes in spatial resolution, contrast resolution and noise. Original image (**a**) can be compared to a smoothed image (**b**), showing reduced spatial resolution (as well as reduced noise), and image with reduced contrast resolution (**c**), and one with artificial noise added (**d**)

be considered as another image quality metric for medical images which involve distance calibration, including CBCT. This section will provide a brief overview of these image quality parameters; information on their assessment during quality control is presented in Chap. 6.

2.5.1.1 Spatial Resolution

Spatial resolution (or sharpness) is the ability to distinguish small details in the image, and can be expressed, for example, as the ability to discriminate two small-sized structures. The spatial resolution of CBCT images is related to, but not exclusively determined by, the *voxel size* (Fig. 2.22). CBCT units nominally provide isotropic (i.e., cubical) voxels, implying that spatial resolution should be approximately the same in all three orthogonal dimensions. The voxel size is thus expressed as the length of any side of the voxel. It should be noted that CBCT images are often displayed using a certain "slice thickness." The use of a slice thickness larger than the voxel size effectively leads to cuboidal voxels, and reduces noise at the cost of a lower spatial resolution in the dimension perpendicular to the slice.

Voxel sizes range between CBCT units and exposure protocols, and are found between 0.07 and 0.6 mm. The small voxel size in CBCT, along with other factors affecting spatial resolution, facilitates its application in dentistry for those tasks requiring high detail, such as the evaluation of root and periapical pathology, ankylosis, root resorption, and impaction.

Apart from the voxel size, spatial resolution of CBCT systems strongly depends on the detector's nominal pixel size and fill factor, although other factors can affect the maximum achievable resolution (e.g., beam projection geometry, X-ray scatter, detector and patient motion, focal spot size, number of basis images, and reconstruction algorithm).

For larger FOV sizes, the reconstructed voxel size cannot be as small as for small FOVs due to computational limitations. However, it is theoretically possible to re-reconstruct all or a part of a large FOV at a smaller voxel size, allowing for an increased spatial resolution. Several manufacturers have implemented this function.

2.5.1.2 Contrast Resolution

Contrast resolution in X-ray imaging can be defined as the ability to discriminate objects of different density (or, specifically, attenuation).

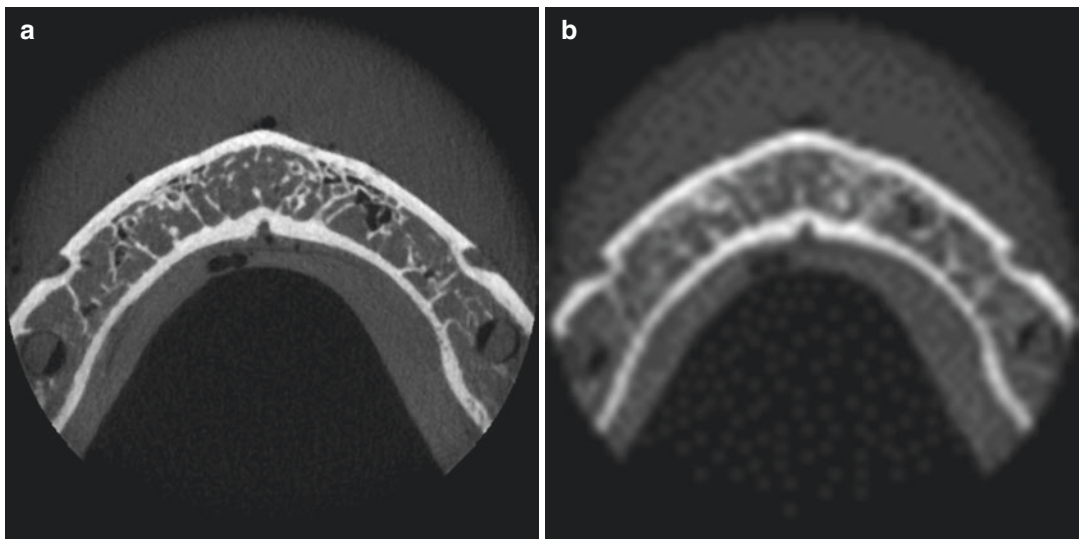

Fig. 2.22 Visual comparison of an original axial CBCT image at a 0.125 mm × 0.125 mm × 0.125 mm voxel size (**a**) and a resampled image at a 1 mm × 1 mm × 0.125 mm voxel size (**b**). The increased voxel size reduces both spatial resolution and noise

Whereas spatial resolution of CBCT is generally considered high compared to MDCT, contrast resolution is limited by numerous factors. The inherent geometric configuration of CBCT results in a high amount of detected scatter radiation. The two main reasons for this are the relatively short object-detector distance and the use of 2D detector panels with no collimation at the detector level. This is a significant factor in reducing the contrast of any CBCT system. In addition, the inherent efficiency, as well as the stability and linearity of the response, is lower for currently used CBCT detectors than for MDCT detectors. For these reasons, as well as the relatively low tube output (i.e., kV and mAs) used in CBCT, CBCT images cannot reveal subtle differences between soft tissues, such as between fluids and solid tumors, and are primarily applied for the visualization of tissues with high anatomical contrast.

2.5.1.3 Noise

Image noise in radiography can be defined as the variability (e.g., standard deviation) of grey values in a homogenous object or tissue. There are various sources of noise in CBCT. As it involves relatively low exposure levels, the random nature of X-ray interactions results in an inhomogeneous signal at the detector (i.e., quantum noise). X-ray scatter, especially when randomly distributed, further adds to the noise of the incoming signal. The detector itself causes electronic noise during signal transmission. Furthermore, filtering during image reconstruction can either suppress or enhance noise (balancing it with spatial resolution).

2.5.1.4 Artifacts

Artifacts in radiography are appearances in the image that do not correspond to the physical reality. While metal artifacts are often most commonly encountered in CBCT, there are various other sources of artifacts.

Metal artifacts are the result of exuberant absorption of X-rays by the metal, and the inability of the reconstruction algorithm to cope with this, leading to dark and bright regions and streaks in the vicinity of the metal. Metal artifacts can severely affect the visibility of structures in the vicinity of, or in-between, metal objects. Therefore, metal objects should be removed prior to scanning if possible (e.g., removable prosthesis). The adjustment of exposure parameters such as kV and mAs has little effect on metal artifacts, and the effect on radiation dose is disproportionate (Pauwels et al. 2013). In addition, current metal artifact reduction techniques in CBCT do not consistently lead to an improvement in diagnostic image quality (Bechara et al. 2012; Bezerra et al. 2015; Kamburoğlu et al. 2013; Parsa et al. 2014). Since metal artifacts manifest primarily in the axial plane because of the X-ray beam geometry, the patient's head can be tilted in some cases to avoid interference of metal artifacts with a certain region of interest.

A relatively common type of artifact in CBCT is due to *patient motion*. The fact that the patient is in a sitting or standing position for most units, along with the relatively long scan time (usually 15–20 s), can result in slight or more severe motion blurring. While slight movements (e.g., swallowing, regular breathing) does not lead to considerable image degradation, excessive movement can lead to severe distortion, possibly requiring retakes (Nardi et al. 2016; Spin-Neto et al. 2013) (Fig. 2.23).

Furthermore, the (lack of) stability of grey values of identical tissues throughout the FOV (i.e., uniformity) can be considered as an image artifact, although it does not necessarily affect the perceived spatial or contrast resolution. Various types of uniformity issues are present in CBCT (Fig. 2.24). Anteroposterior shading can occur for small or noncentrally positioned FOVs in particular, due to the effect of tissues outside the FOV (Siltanen et al. 2003). Central-to-peripheral grey value gradients, known as *cupping and doming* (or '*capping*') artifacts, also commonly occur in CBCT due to the effect and overcorrection, respectively, of beam hardening.

Furthermore, ring artifacts can occur due to improper detector calibration, as any detector pixel giving a consistently overestimated or

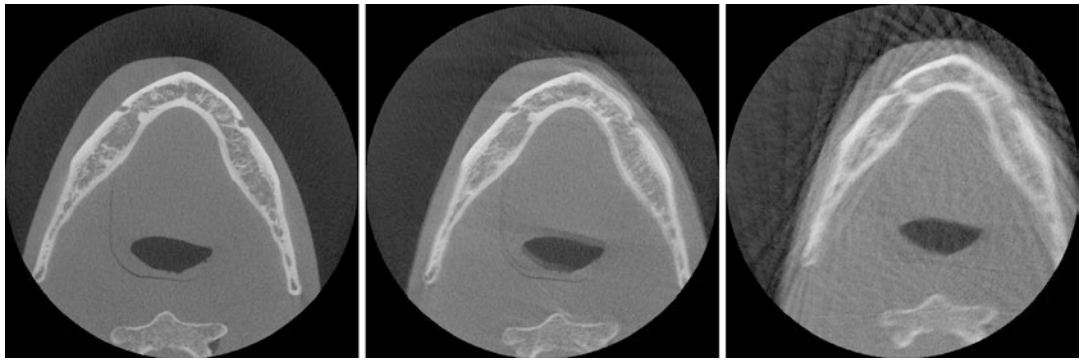

Fig. 2.23 Axial slices of CBCT scans of an anthropomorphic phantom, illustrating the effect of motion during CBCT acquisition. *left*: stationary phantom. *middle*: moderate motion. *right*: severe motion

underestimated read-out value will manifest itself as a circle on the reconstructed image.

2.5.1.5 Geometric Accuracy

The geometric accuracy of CBCT can be expressed as the accuracy of linear, area, and volume measurements. It is affected by the spatial resolution of the image, the accuracy of geometric calibration, and the presence of geometric distortion.

- **Spatial resolution—partial volume averaging.** The accuracy of a measurement partially relies on the ability to identify the boundaries of the measured structure. Images with poor resolution suffer from an effect known as partial volume averaging, in which the edges between different tissues are not properly represented (Fig. 2.25). This can lead to deviations in manual or automatic measurements.
- **Geometric calibration.** As CBCT images are calibrated for absolute distance measurements, it is essential that the voxel size correctly represents the actual physical size. Over- or underestimation of the voxel size can lead to consistent measurement deviations.
- **Geometric distortion.** Image intensifier-based CBCT units were prone to geometric distortion such as the pincushion effect. Flat panel CBCTs are less susceptible to geometric distortion, although it may still occur, e.g., due to deviations in tube/detector rotation from a perfect circular trajectory (and improper compensation thereof).

2.5.2 Exposure Parameters

Several exposure parameters determine the energy and quantity of the X-ray beam as well as the quality of the projection image. Some of the factors, such as focal spot size, source-object distance, object-detector distance, beam filtration, and beam frequency, are equipment-dependent and cannot be altered by the operator. Others, such as milliamperage (mA), exposure time (s), and kilovoltage (kV), can be operator-controlled within a certain range, depending on the CBCT model.

2.5.2.1 Equipment-Dependent Factors

- **Focal Spot Size.** The focal spot is the area at the anode which is hit by the electron beam, leading to the production of X-rays. The focal spot determines the penumbra or geometric unsharpness of the projection images, seeing that the reconstruction algorithm assumes that all X-rays originate from an infinitely small point source. Smaller focal spot sizes result in a smaller penumbra and theoretically sharper images (Fig. 2.26). Most CBCT units have a nominal focal spot of 0.5 mm, although smaller focal spots are used by some models. When using a smaller focal spot, care has to

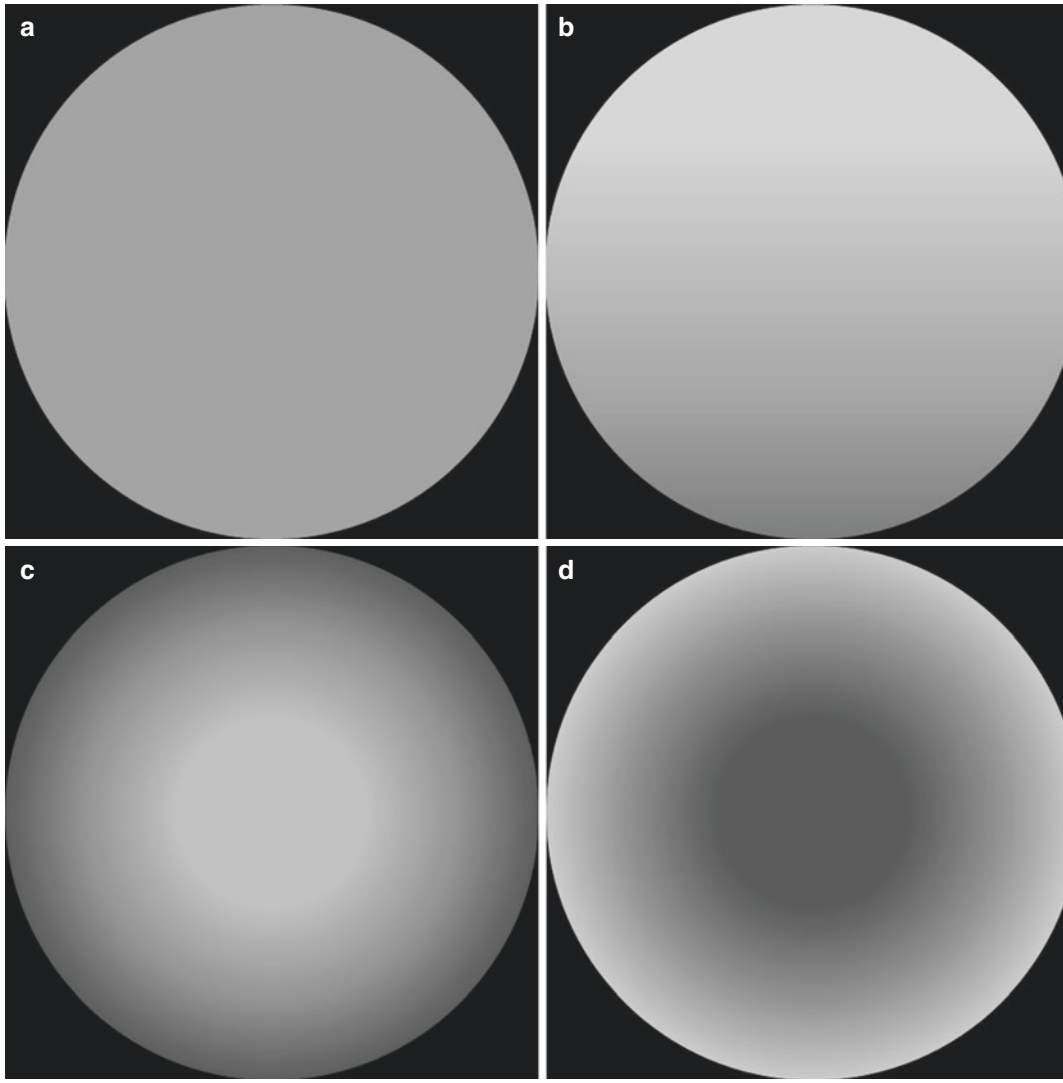

Fig. 2.24 Simulated images representing axial CBCT slices of a homogeneous object of water-equivalent (or similar) density demonstrating grey value uniformity issues encountered within the FOV for CBCT. Perfect uniformity (**a**) demonstrates homogeneous grey values throughout the image as compared with images showing anteroposterior shading (**b**), capping/doming artifact (**c**), and cupping artifact (**d**)

be taken to avoid overheating and damaging of the anode (e.g., by reducing the kV or mAs or increasing the cool-down time between consecutive exposures).

- **Source-Object Distance (SOD) and Object-Detector distance (ODD).** A shorter SOD increases the penumbra (Fig. 2.26) and results in a higher local skin exposure at the entrance point of the beam. However, a shorter SOD increases geometric magnification of the projection image. A longer SOD and/or shorter ODD decreases the penumbra and allows for the use of smaller detectors (Fig. 2.26); however, the proportion of detected X-ray scatter, which deteriorates image quality, increases at a shorter ODD. For very short ODDs, there is a higher risk of the patient's shoulder interfering with the rotational motion, especially that of the detector. This can be negated by the manufacturer by slightly tilting the detector or

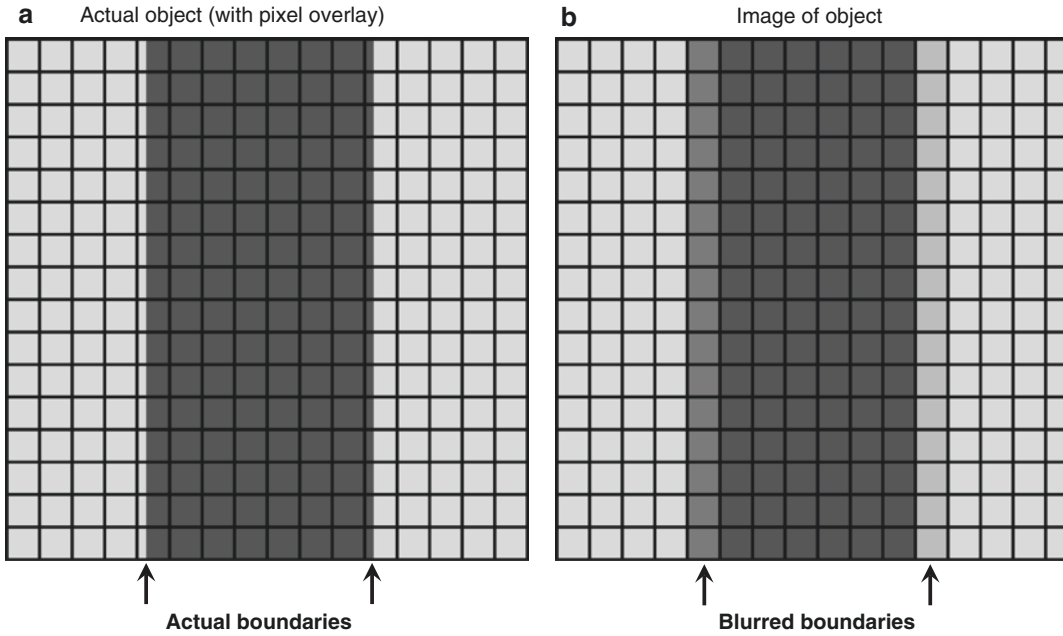

Fig. 2.25 Two-dimensional schematic representation demonstrating partial volume averaging. If an image pixel matrix is layered over an object (**a**) it is possible that the boundary between the object and the pixel matrix does not coincide. When this occurs, the grey value in the pixel containing the boundary will represent the volume-averaged attenuation of the materials comprising it, resulting in a blurring of the boundary in the image of the object (**b**). In actual radiographic images, blurring is further enhanced due to other factors (e.g., focal spot size, motion blur)

by the operator by performing a collision check (rotating the C-arm without exposure) before image acquisition.

- **Beam Filtration.** Before exiting the tube, X-ray beams are filtered by both the tube housing and a thin sheet of metal (e.g., aluminum, copper). This is done to remove the low-energy X-ray photons from the beam, as they are more susceptible for photoelectric absorption than high-energy X-rays. Low-energy photons are not of use for diagnostic imaging, as they are very likely to be absorbed in the patient (contributing to the radiation dose, but not contributing to image formation). Furthermore, the patient also acts as a filter, which can lead to beam hardening artifacts in CBCT, especially in the presence of high-density material (see Sect. 2.5.1.4). Increased filtration at the X-ray tube "pre-hardens" the beam (i.e., increases its mean energy), leading to greater dose efficiency and reduced beam hardening artifacts, but also reduces the total beam intensity. Therefore, there is a limit as to how much the beam can be filtered while still being able to reach a sufficient detector signal at an acceptable tube load. The minimum beam filtration is determined by international standards; the actual beam filtration can vary between CBCT models. While flat filters result in uniform beam filtration, other filter shapes (e.g., bowtie) can be used to reduce beam uniformity issues such as the heel effect.
- **X-ray Frequency.** Technically, the simplest method of acquiring images in a single rotational scan is to use a constant beam of radiation and to allow the X-ray detector to sample the attenuated beam during its trajectory. Alternatively, the X-ray beam may be pulsed to coincide with the detector activation or sampling. The latter approach results in a reduced overall exposure time and, as a result, a lower patient radiation exposure. It also reduces the impact of detector afterglow such that the number of frames acquired per second can, to some

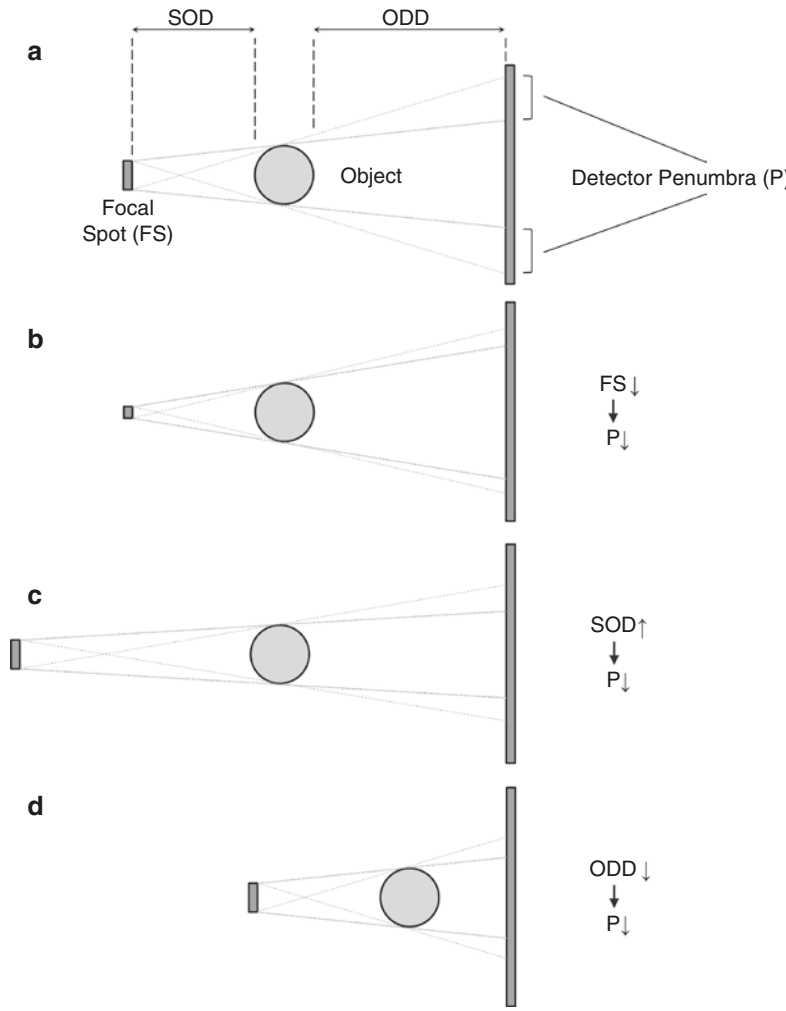

Fig. 2.26 Schematic representation of the effect of focal spot (FS) size, source-object distance (SOD) and object-detector distance (ODD) on image penumbra (**a**). A smaller focal spot size (**b**), larger SOD (**c**) and smaller ODD (**d**) all decrease the penumbra width, which increases image sharpness. (Figure reproduced from Pauwels et al. (2015a) under the British Institute of Radiology's License to Publish)

extent, be increased, which leads to faster rotation times and potentially reduced motion artifacts. In addition, pulsed systems result in substantially reduced tube load; therefore, less cool-down time is necessary between patients. On the other hand, the use of continuous exposure can result in a more homogenous tube output throughout the time in which a projection is acquired. The use of pulsed exposure requires recurrent on and off switching of the tube voltage, which coincides with a certain build-up and shut-down period in which tube voltage is between 0 and the peak kV. If the projection windows (partly) cover these two lag periods, image quality can be affected. In dental CBCT, pulsed exposures are used by most models; thus, the exposure time is often much lower than the scan time. The frequency and duration of pulsing, however, varies between CBCT units. The effect of pulsed exposure on dose efficiency (i.e., radiation dose vs. image quality) has not yet been definitively addressed.

2.5.2.2 Operator-Dependent Factors

The available ranges of exposure factors in CBCT greatly depend on the manufacturer. Whereas some manufacturers allow for a limited selection of exposure protocols, others allow for manual adjustment of exposure settings within a certain range. While the former is a more user-friendly approach, the latter allows for increased patient-specific dose optimization, providing that

the user understands the effects of each parameter on image quality and radiation dose. It is essential to select exposure settings or protocols yielding the lowest possible dose for a given patient according to the *ALARA* (As Low As Reasonably Achievable) principle.

- **Milliamperage (mA).** The mA determines the number of X-rays exiting the tube per unit time. The mA required for a diagnostically acceptable image is coupled with the kV and exposure time; thus, CBCT units have shown wide ranges in terms of mA. The radiation dose increases proportionately with the mA at a 1:1 ratio. In terms of image quality, a higher mA results in an increased detector signal which reduces image noise (Fig. 2.27). In clinical practice, mA should be varied with

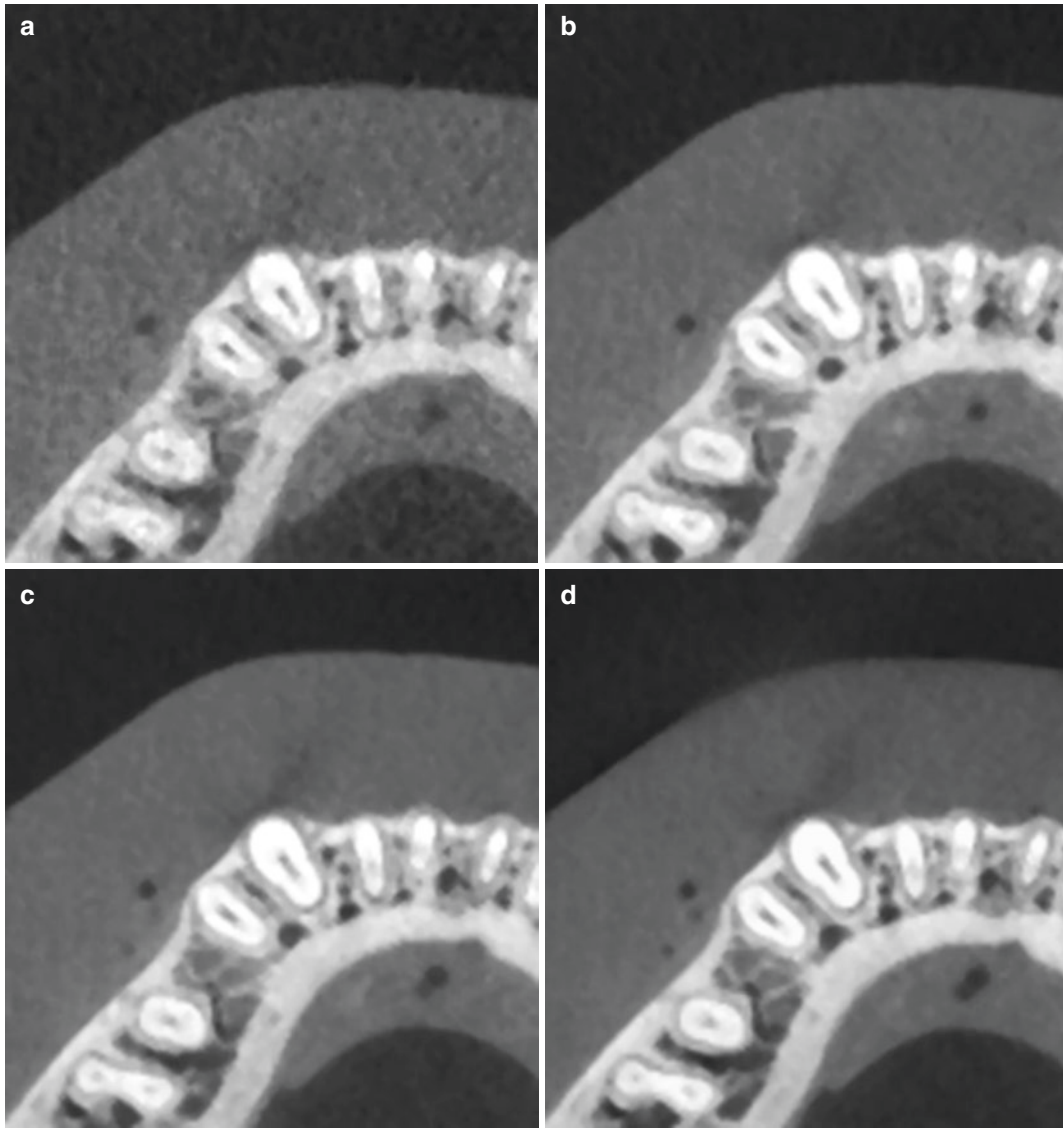

Fig. 2.27 Cropped (*right*) axial images of the right anterior mandible of an anthropomorphic phantom scanned at 1 mA (**a**), 3 mA (**b**), 5 mA (**c**), and 7 mA (**d**) exposure (3D Accuitomo 170, J. Morita, Kyoto, Japan) operating at 90 kV, and 17.5 s exposure time. At lower exposure levels, there is a clear effect of mA on noise, depicted as graininess. The effect diminishes at higher exposure levels

patient size, with smaller patients (e.g., children) requiring a lower mA to reach the same image quality as larger patients (Pauwels et al. 2017). Furthermore, the mA (or other exposure parameters) can be adjusted to the diagnostic task, with certain clinical indications (e.g., implant planning) requiring a lower image quality level than others (e.g., endodontic evaluation).

- **Kilovoltage (kV).** Adjustment of kV has a more complicated effect on radiation dose than that of mA. An increase in kV leads to a greater number of X-rays per unit time, but also increases the mean and maximum energy of these X-rays. The relationship between kV and dose is approximately quadratic within the diagnostic energy range. An increase in voltage from 60 to 90 kV can triple the radiation dose if all other exposure parameters remain the same (Pauwels et al. 2014). In terms of image quality, a higher kV reduces image noise and beam hardening, but affects contrast as well through an interplay between X-ray scatter (Compton and Rayleigh scatter, both of which are kV-dependent) and beam penetration (which increases with the kV) (Fig. 2.28). Most CBCT units operate at or below 90 kV, whereas a few can operate at higher kVs, up to 120 kV. In general, low-kV units operate at a higher mA. This lack of standardization indicates that the most dose-efficient combination of kV and mA in CBCT imaging has not yet been determined.

2.5.3 Projection Images

The number of projections acquired during a CBCT scan is determined by the frame rate (number of projections acquired per second), the extent of the rotation arc (180°–360°), and the speed of the rotation.

- **Exposure time (s)**. In CBCT, whether or not pulsed exposure is used, the exposure time is proportionate to the number of acquired projections. Typically, a few discrete options in terms of exposure time are available. Units using pulsed exposure have a lower exposure time for a given number of projections than those with continuous exposure.
- **Frame Rate.** Higher frame rates allow for shorter scan time, which can lead to images with less artifacts and better image quality. High frame rates require detectors with pixels sensitive enough to reach an adequate signal-to-noise ratio during a short time frame.

In CBCT, the number of projections typically ranges between 150 and 1000. While the use of too few projections results in aliasing artifacts due to undersampling (Fig. 2.29), this is not seen during normal CBCT use. An increased number of projections provides more information to reconstruct the image, resulting in a decreased image noise (Fig. 2.30). An increased number of projections would therefore allow the image to be reconstructed at a smaller voxel size while keeping

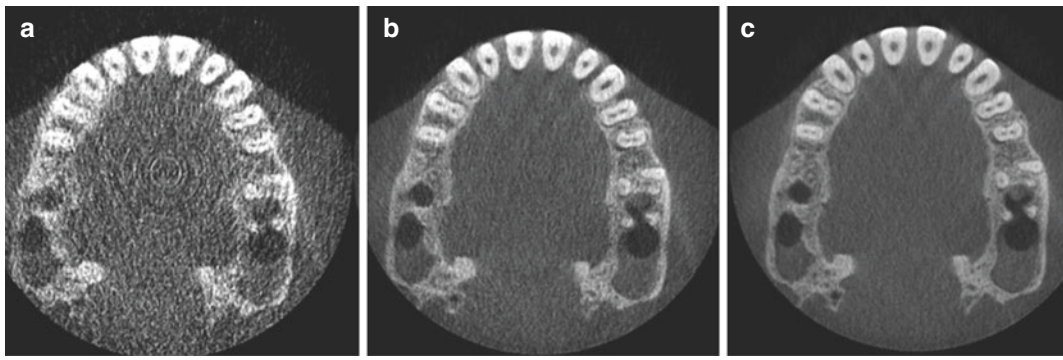

Fig. 2.28 Axial images of a plastic encased skull at (**a**) 60 kv, (**b**) 75 kV and (**c**) 90 kV acquired on a 3D Accuitomo 170 (J. Morita, Kyoto, Japan) operating at 5 mA, and 17.5 s exposure time, showing the effect of increasing kilovoltage on image quality, such as noise (Courtesy of William C. Scarfe)

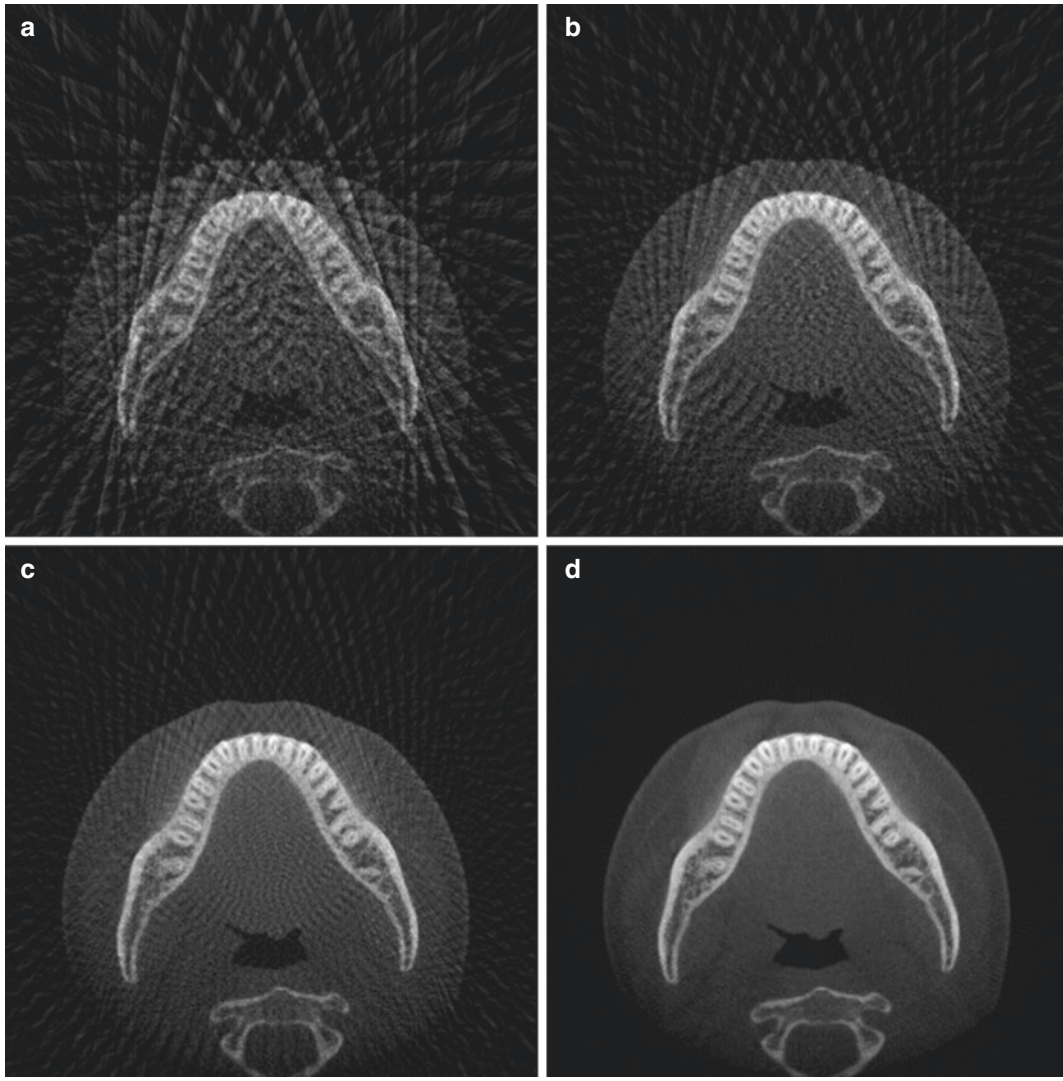

Fig. 2.29 Simulated FBP reconstruction of an axial slice using (**a**) 18 (**a**), 36 (**b**), 60 (**c**), and 180 projections (**d**). As the number of frames increases so does the exposure time and therefore radiation dose to the patient

noise at a reasonable level, effectively increasing spatial resolution. Therefore, the choice between a low or high number of projections (i.e., a short or long exposure time) is often coupled with larger or smaller voxel sizes, respectively; thus, imaging protocols with relatively short and long exposure times are often referred to as low- and high-resolution protocols. The user should adapt the number of projections to the patient, mainly depending on the spatial resolution required by the clinical indication at hand. It should be taken into account that a larger number of projections coincides with a longer scan time, a proportionately higher patient dose, an increased lag time between patients to allow for cooling of the generator tube and a longer reconstruction time. In addition, patient motion can be more severe, leading to potential image blurring and artifacts.

2.5.4 Rotation Angle

As one can imagine from Fig. 2.13, projections from opposing angles are redundant, as the back-projection would be identical (although this is not entirely the case when a divergent beam does not

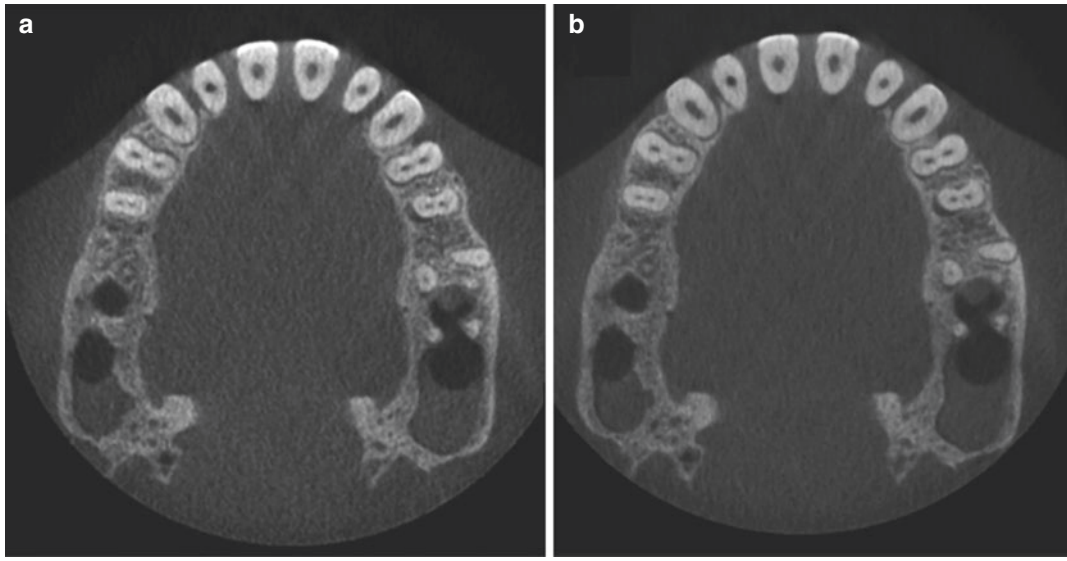

Fig. 2.30 Axial CBCT images of a plastic encased skull (3D Accuitomo 170, J. Morita, Kyoto, Japan) acquired at 5 mA and 512 (**a**) and 1024 (**b**) projection images, showing the effect of increasing number of basis projections on noise. (Courtesy of William C. Scarfe)

fully cover the diameter of the scanned object; see Sect. 2.2.1.2). While many CBCT units acquire projections over a rotation arc of 360°, a shorter rotation would theoretically suffice. As with any change in exposure time, the use of a shorter rotation arc decreases patient dose and potentially reduces motion blurring at the cost of an increased image noise (Fig. 2.31). In some cases, the use of a partial rotation is done for practical reasons, as it allows the unit to be more compact (e.g., hybrid CBCT-panoramic systems). Certain units allow the user to choose between a full or partial rotation.

2.5.5 Field of View

The dimensions of the FOV, or scan volume, are primarily dependent on the detector size and the beam projection geometry (e.g., source-object and object-detector distance). The shape of the scan volume can be either cylindrical (pyramid-shaped X-ray beam) or spherical (cone-shaped X-ray beam). As discussed in Chap. 7, collimation of the primary X-ray beam can considerably reduce patient radiation dose and is an essential technique for dose optimization. The FOV should be minimized according to the region of interest corresponding to the diagnostic task.

Reduction in the FOV usually can be accomplished mechanically or, in some instances, electronically. Currently, most CBCT units use adjustable metallic shields acting as primary collimation at the radiation source. Electronic collimation involves elimination (i.e., cropping) of projection data in order to reduce the reconstructed image to the area of interest. Both techniques reduce the computational time during reconstruction, but only physical collimation results in reduced patient dose collimation should be strongly discouraged.

Effects of FOV size on image quality can be seen in some cases. Larger FOVs increase the amount of scatter per detector area, reducing image quality (Pauwels et al. 2016). In addition, larger FOVs coincide with a higher beam divergence at the edge of the FOV, which results in image quality deterioration. On the other hand, a FOV with a larger diameter reduces the "local tomography" effect, which is the effect of tissue outside the FOV (which is only partially exposed) on grey value uniformity (Siltanen et al. 2003).

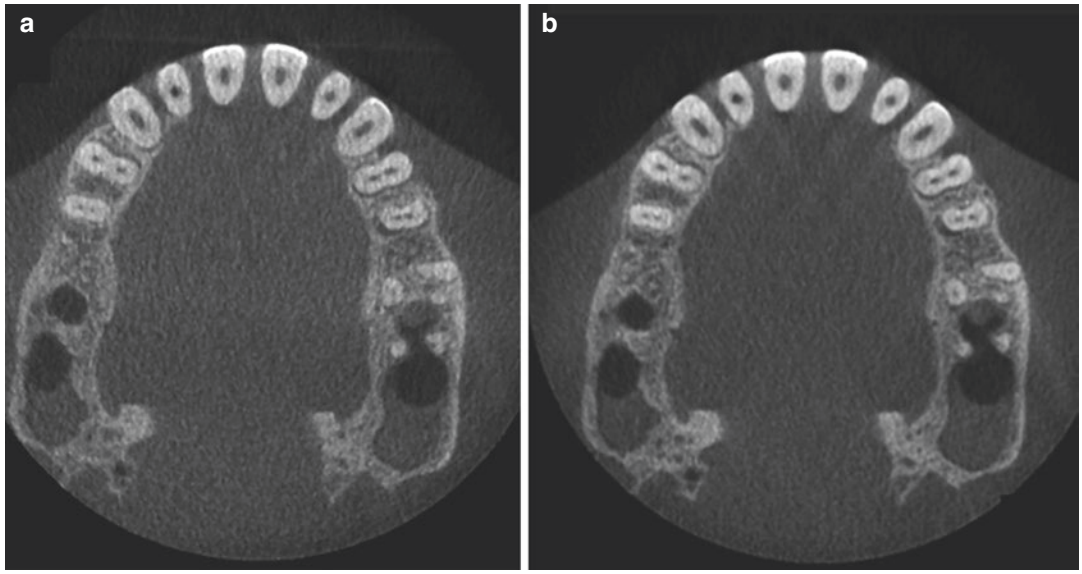

Fig. 2.31 Axial and cross-sectional CBCT images of a plastic encased skull (3D Accuitomo 170, J. Morita, Kyoto, Japan) acquired at 90 kV, 5 mA, and 180° (**a**) and 360° (**b**) rotational angle, showing the effect of rotation angle on noise

2.6 Future Technical Developments

Several technical developments in terms of CBCT image acquisition and reconstruction can be expected in the near future. Most of these are already applied in MDCT imaging pre-clinically or clinically.

The use of dual energy imaging in MDCT has led to dramatic improvements in terms of tissue characterization, in some cases avoiding the need for contrast media. Typically, this involves an overlapping image acquisition using 2 kV settings (either by the same X-ray generator, or separate sources) (Karçaaltıncaba and Aktas 2011). Dual energy imaging allows for a greater contrast resolution, although it is not yet clear if it would be cost-efficient for dental and maxillofacial CBCT.

A technique which has been implemented in MDCT imaging for several years is the use of automatic exposure control (AEC). Various levels and methods of AEC exist; the main principle is the adjustment of tube output (typically the mA) according to the size and density distribution of the object under investigation (Alibek et al. 2011). While a slice-by-slice AEC is obviously not feasible in CBCT, seeing that the entire volume is acquired in one rotation, the application of AEC could still lead to considerable dose reduction. First of all, it would enable a constant image quality between patients of different sizes, without the need for manual adjustment of exposure parameters. Secondly, AEC could be applied during an image acquisition, seeing that the detector signal varies considerably between lateral projection angles and A-P or P-A angles. If the tube output could automatically be adjusted throughout the scan depending on the amount and density of the traversed tissue (i.e., using real-time feedback of the acquired projections), the dose for each projection would be minimized.

Several innovations at the level of the detector are also currently under investigation, or expected in the near future. General improvements to FPDs (e.g., sensitivity, frame rate, uniformity, electronic noise) could lead to considerable improvements in terms of dose efficiency. On the other hand, CBCT could evolve towards the use of photon counting or energy-resolving detectors, which could lead to an improvement in terms of image quality, especially when coupled with dedicated reconstruction techniques.

It can be expected that image reconstruction algorithms will evolve from the currently used FDK technique to iterative reconstruction. Iterative reconstruction techniques, which are a class of reconstruction techniques involving multiple rounds ("iterations") of image reconstruction (see Fig. 2.18), have resulted in noise and artifact reduction in clinical MDCT imaging (Korn et al. 2012), and are expected to become more widely used in CBCT.

A more challenging innovation is the use of X-ray phase-contrast (Pfeiffer et al. 2008). Currently, X-ray imaging is based on attenuation. However, X-rays also exhibit a phase shift while passing through matter, which is currently ignored because it cannot be detected using conventional X-ray sensors. The use of phase-contrast would lead to a much improved contrast in the soft tissue density range. While phase-contrast imaging is in a relatively early stage, 2D and 3D imaging modalities based on phase-contrast could change the paradigm of X-ray imaging at some point.

Acknowledgments 3D head model images in Figs. 2.10, 2.17, and 2.20 are courtesy of Rodrigue Pralier. Figures 2.1, 2.2, 2.3, 2.4, 2.1, and 2.25 are partially adapted from Pauwels et al. (2015a) under the British Institute of Radiology's License to Publish. Images used in Fig. 2.19 are courtesy of J. Morita, Osaka, Japan.

References

Alibek S, Brand M, Suess C, Wuest W, Uder M, Greess H (2011) Dose reduction in pediatric computed tomography with automated exposure control. Acad Radiol 18:690–693

Bechara BB, Moore WS, McMahan CA, Noujeim M (2012) Metal artefact reduction with cone beam CT: an in vitro study. Dentomaxillofac Radiol 41:248–253

Beister M, Kolditz D, Kalender WA (2012) Iterative reconstruction methods in X-ray CT. Phys Med 28:94–108

Bezerra IS, Neves FS, Vasconcelos TV, Ambrosano GM, Freitas DQ (2015) Influence of the artefact reduction algorithm of Picasso Trio CBCT system on the diagnosis of vertical root fractures in teeth with metal posts. Dentomaxillofac Radiol 44:20140428

Birch R, Marshall M (1979) Computation of bremsstrahlung X-ray spectra and comparison with spectra measured with a Ge(Li) detector. Phys Med Biol 24:505–517

Feldkamp LA, Davis LC, Kress JW (1984) Practical cone-beam algorithm. J Opt Soc Am A 1:612–619

Kamburoğlu K, Kolsuz E, Murat S, Eren H, Yüksel S, Paksoy CS (2013) Assessment of buccal marginal alveolar peri-implant and periodontal defects using a cone beam CT system with and without the application of metal artefact reduction mode. Dentomaxillofac Radiol 42:20130176

Karçaaltıncaba M, Aktas A (2011) Dual-energy CT revisited with multidetector CT: review of principles and clinical applications. Diagn Interv Radiol 17:181–194

Korn A, Fenchel M, Bender B, Danz S, Hauser TK, Ketelsen D, Flohr T, Claussen CD, Heuschmid M, Ernemann U, Brodoefel H (2012) Iterative reconstruction in head CT: image quality of routine and low-dose protocols in comparison with standard filtered back-projection. AJNR Am J Neuroradiol 33:218–224

Loubele M, Jacobs R, Maes F, Schutyser F, Debaveye D, Bogaerts R, Coudyzer W, Vandermeulen D, van Cleynenbreugel J, Marchal G, Suetens P (2005) Radiation dose vs. image quality for low-dose CT protocols of the head for maxillofacial surgery and oral implant planning. Radiat Prot Dosim 117:211–216

Loubele M, Bogaerts R, Van Dijck E, Pauwels R, Vanheusden S, Suetens P, Marchal G, Sanderink G, Jacobs R (2009) Comparison between effective radiation dose of CBCT and MSCT scanners for dentomaxillofacial applications. Eur J Radiol 71:461–468

Molteni R (2013) Prospects and challenges of rendering tissue density in Hounsfield units for cone beam computed tomography. Oral Surg Oral Med Oral Pathol Oral Radiol 116:105–119

Nardi C, Molteni R, Lorini C, Taliani GG, Matteuzzi B, Mazzoni E, Colagrande S (2016) Motion artefacts in cone beam CT: an in vitro study about the effects on the images. Br J Radiol 89:20150687

Nemtoi A, Czink C, Haba D, Gahleitner A (2013) Cone beam CT: a current overview of devices. Dentomaxillofac Radiol 42:20120443

Pauwels R, Stamatakis H, Bosmans H, Bogaerts R, Jacobs R, Horner K, Tsiklakis K, SEDENTEXCT Project Consortium (2013) Quantification of metal artifacts on cone beam computed tomography images. Clin Oral Implants Res 24(Suppl A100):94–99

Pauwels R, Silkosessak O, Jacobs R, Bogaerts R, Bosmans H, Panmekiate S (2014) A pragmatic approach to determine the optimal kVp in cone beam CT: balancing contrast-to-noise ratio and radiation dose. Dentomaxillofac Radiol 43:20140059

Pauwels R, Araki K, Siewerdsen JH, Thongvigitmanee SS (2015a) Technical aspects of dental CBCT: state of the art. Dentomaxillofac Radiol 44:20140224

Pauwels R, Jacobs R, Bogaerts R, Bosmans H, Panmekiate S (2016) Reduction of scatter-induced image noise in cone beam computed tomography: effect of field of view size and position. Oral Surg Oral Med Oral Pathol Oral Radiol 121:188–195

Pauwels R, Jacobs R, Bogaerts R, Bosmans H, Panmekiate S (2017) Determination of sizespecific exposure settings in dental cone-beam CT. Eur Radiol 27:279–285

Pfeiffer F, David C, Bunk O, Donath T, Bech M, Le Duc G, Bravin A, Cloetens P (2008) Region-of-interest tomography for grating-based X-ray differential phase-contrast imaging. Phys Rev Lett 101:168101

Parsa A, Ibrahim N, Hassan B, Syriopoulos K, van der Stelt P (2014) Assessment of metal artefact reduction around dental titanium implants in cone beam CT. Dentomaxillofac Radiol 43:20140019

Seibert JA (2006) Flat-panel detectors: how much better are they? Pediatr Radiol 36:173–181

Siltanen S, Kolehmainen V, Järvenpää S, Kaipio JP, Koistinen P, Lassas M, Pirttilä J, Somersalo E (2003) Statistical inversion for medical x-ray tomography with few radiographs: I. General theory. Phys Med Biol 48:1437–1463

Spin-Neto R, Mudrak J, Matzen LH, Christensen J, Gotfredsen E, Wenzel A (2013) Cone beam CT image artefacts related to head motion simulated by a robot skull: visual characteristics and impact on image quality. Dentomaxillofac Radiol 42:32310645